Dynamic Response, Residual Strength, and High Strain-Rate Failure Modes of Rock and Concrete

FINAL TECHNICAL REPORT

01 August 1996 – 31 October 1999

GRANT NO. AFOSR F49620-96-1-0393

to

University of California, San Diego

by

Air Force Office of Scientific Research

Principal Investigator: **Dr. Sia Nemat-Nasser**

Center of Excellence for Advanced Materials
Department of Mechanical and Aerospace Engineering
University of California, San Diego
9500 Gilman Drive
La Jolla, CA 92093-0416

Submitted April 15, 2000

SF 298 MASTER COPY KEEP THIS COPY FOR REPRODUCTION PURPOSES

2000

REPORT DOCUMENTATION PAGE

AFRL-SR-BL-TR-00-

0789

1. AGENCY USE ONLY *(Leave blank)*	2. REPORT DATE	3. REPORT TYPE AND DATES COVERED
		Final Technical Report 8/1/96-10/31/99

4. TITLE AND SUBTITLE
Dynamic Response, Residual Strength, and High Strain-Rate Failure Modes of Rock and Concrete

5. FUNDING NUMBERS

6. AUTHOR(S)
Dr. Sia Nemat-Nasser

7. PERFORMING ORGANIZATION NAMES(S) AND ADDRESS(ES)
Center of Excellence for Advanced Materials
Department of Applied Mechanics and Engineering Science
University of California, San Diego
9500 Gilman Drive, La Jolla, CA 92093-0416

8. PERFORMING ORGANIZATION REPORT NUMBER

9. SPONSORING / MONITORING AGENCY NAME(S) AND ADDRESS(ES)
Dr. Steven Walker
AFOSR/NA
801 North Randolph Street, Room 732
Arlington, VA 22203-1977

10. SPONSORING / MONITORING AGENCY REPORT NUMBER
F49620-96-1-0393

11. SUPPLEMENTARY NOTES
04-20-00P03:07 RCVD

The views, opinions and/or findings contained in this report are those of the author(s) and should not be construed as an official Department of the Army position, policy or decision, unless so designated by other documentation.

12a. DISTRIBUTION / AVAILABILITY STATEMENT
Approved for public release; distribution unlimited.

12 b. DISTRIBUTION CODE

13. ABSTRACT *(Maximum 200 words)*

At UCSD, we have initiated a fundamental research program in order to understand and quantify the dynamic response and failure modes of rocks and concrete, using a coordinated effort which involves material characterization, high-strain-rate experiments, and physically-based analytical-computational modeling. The work includes the following major tasks: I. Microstructural Characterization (I.1: Ultrasonic Measurements; I.2: Microscopy; I.3: Image Processing; I.4: Statistical Measures), II. Mechanical Tests (II.1: Quasi-static Experiments; II.2: Hopkinson Bar Experiments; II.3: Gas Gun Experiments), III. Model Experiments, IV. Physically-based Modeling, and V. Verification of Model Predictions.

The research includes a set of carefully designed recovery experiments using UCSD's 2.5- and 6-inch gas guns and the 1.5- and 3-inch Hopkinson bars; the mechanisms and nature of shock-induced damage in the material are being studied. The strain rate, stress amplitude, and the total input energy are controlled in these tests. Both jacketed and unjacketed samples are used. Through the use of ultrasonic measurements, the degradation in the sample stiffness will be measured nondestructively. These measurements will then be correlated with microscopic observations of the specimens, using optical microscopy and SEM. Based on the knowledge gained through the above experimental observations, a set of new experiments is planned to study the residual strength and dynamic response of shocked materials. Once the dominant microstructural features are identified, model experiments will be designed to directly examine the damage evolution process.

14. SUBJECT TERMS	15. NUMBER IF PAGES
Dynamic Failure, rock, cement	40
	16. PRICE CODE

17. SECURITY CLASSIFICATION OR REPORT	18. SECURITY CLASSIFICATION OF THIS PAGE	19. SECURITY CLASSIFICATION OF ABSTRACT	20. LIMITATION OF ABSTRACT
UNCLASSIFIED	UNCLASSIFIED	UNCLASSIFIED	UL

1. OBJECTIVES OF RESEARCH

At UCSD, we have initiated a fundamental research program in order to understand and quantify the dynamic response and failure modes of rocks and concrete, using a coordinated effort which involves material characterization, high-strain-rate experiments, and physically-based analytical-computational modeling. The work included major tasks, as indicated in Chart 1.

Our work included a set of carefully designed recovery experiments using UCSD's 2.5- and 6-inch gas guns and the 1.5- and 3-inch Hopkinson bars; the mechanisms and nature of shock-induced damage in the material are being studied. The strain rate, stress amplitude, and the total input energy are controlled in these tests. Both jacketed and unjacketed samples are used. Through the use of ultrasonic measurements, the degradation in the sample stiffness will be measured nondestructively. These measurements will then be correlated with microscopic observations of the specimens, using optical microscopy and SEM. Statistical measures of the microstructural changes will be established, using image-processing techniques. The main objective at this stage of the research is to clearly identify the microstructure prior to dynamic loading and at various stages of the damage evolution, in order to understand the physics of: (1.) microcrack nucleation, growth, interaction, and coalescence; (2.) plastic deformation by dislocation motion, intergranular slip, twinning, and void collapse; and (3.) effects of high strain rate, stress amplitude, and total energy input on the nature and extent of the induced damage.

Based on the knowledge gained through the above experimental observations, a set of new experiments is planned to study the residual strength and dynamic response of shocked materials. Here, the sample geometry and the parameters of the input shock will be adjusted, such that shocked samples with different degrees of damage are obtained. These experiments will be done, using the 6-inch gas gun. The shocked samples will then be characterized, and from them, samples will be prepared for further testing. The aims of this second set of experiments are: 1. to quantify the residual strength and relate it to the preshocked microstructure and the parameters which characterize the shock loading conditions; and 2. to identify the failure modes and the failure micromechanisms of the preshocked materials.

Once the dominant microstructural features are identified, model experiments will be designed to directly examine the damage evolution process. Using transparent samples which contain predesigned defects, high strain-rate microcracking and other related inelastic processes will be recorded by high-speed photography.

Based on our experimental observations, we are now developing a physically-based micromechanical to predict the dynamic response and failure modes of both preshocked and unshocked materials. The predictive capability of these material-response models and the range of their applicability will be tested by *independent* controlled dynamic experiments.

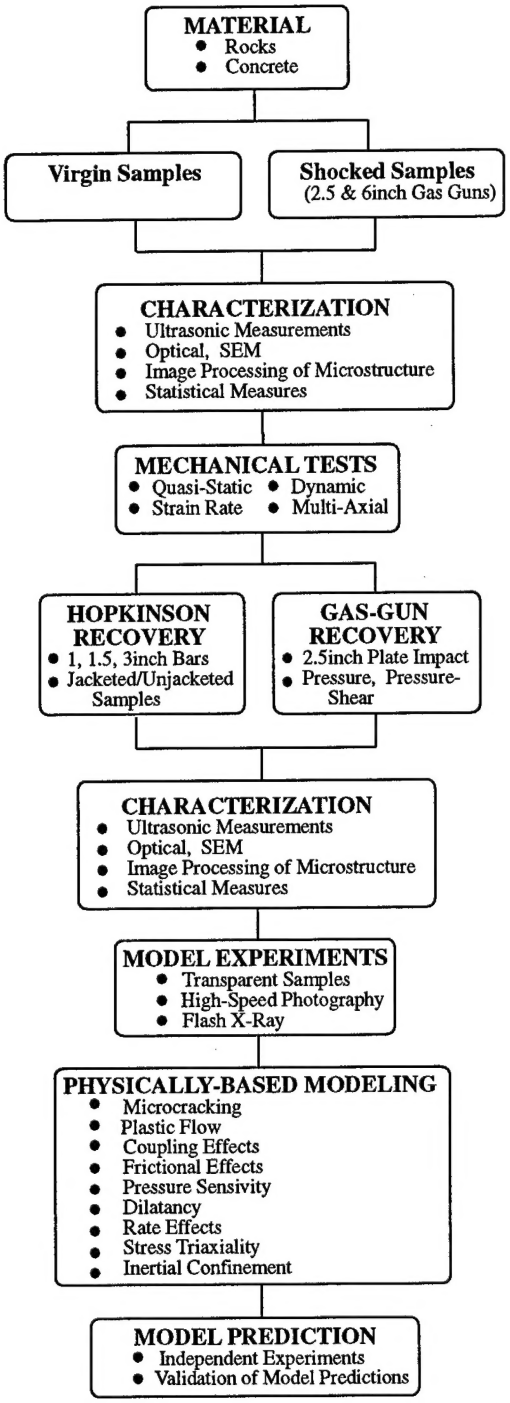
MATERIAL
Rocks
Concrete
Virgin Samples
Shocked Samples
(2.5 & 6inch Gas Guns)
CHARACTERIZATION
Ultrasonic Measurements
Optical, SEM
Image Processing of Microstructure
Statistical Measures
MECHANICAL TESTS
Quasi-Static
Dynamic
Strain Rate
Multi-Axial
HOPKINSON RECOVERY
1, 1.5, 3inch Bars
Jacketed/Unjacketed Samples
GAS-GUN RECOVERY
2.5inch Plate Impact
Pressure, Pressure-Shear
CHARACTERIZATION
Ultrasonic Measurements
Optical, SEM
Image Processing of Microstructure
Statistical Measures
MODEL EXPERIMENTS
Transparent Samples
High-Speed Photography
Flash X-Ray
PHYSICALLY-BASED MODELING
Microcracking
Plastic Flow
Coupling Effects
Frictional Effects
Pressure Sensivity
Dilatancy
Rate Effects
Stress Triaxiality
Inertial Confinement
MODEL PREDICTION
Independent Experiments
Validation of Model Predictions

Chart 1

2. STATUS OF RESEARCH EFFORT ..... see pages 8-32

3. PROFESSIONAL PERSONNEL ASSOCIATED WITH RESEARCH EFFORT AND DEGREES AWARDED

Principal Investigator:	S. Nemat-Nasser
Postdoctoral Research Associates:	None
Visiting Scholars:	None
Graduate Student:	Jacob Rome
Degree Awarded:	Masters - Engr Sciences (Mechanical Engineering), Spring 1997.

4. PUBLICATIONS:

Work in Progress:

"New Experimental Techniques of High-Strain Rate Testing of Concrete"
Jacob Rome and Sia Nemat-Nasser

Abstract:
We have adapted old techniques and developed new techniques to study the dynamic response of concrete. Concrete was tested at high strain rates using the Split Pressure Hopkinson Bar (SPHB), also known as the Kolsky Bar. The samples were tested in both uniaxial and biaxial compression. Further, on many uniaxial tests, high speed photography was employed to observe the loading and unloading process in the samples. Microscopy and other visual methods were employed to observe the concrete after biaxial tests.

5. INTERACTIONS (COUPLING ACTIVITIES)

5.1 PARTICIPATION OF PRINCIPAL INVESTIGATOR AT MEETINGS: PAPERS PRESENTED, LECTURES AND SEMINARS

UCSD's IMM Fourth Summer School, Lecture presented "Micromechanics Approach to Damage", July 22 - August 2, 1996.

1996 IUTAM 19th International Congress of Theoretical and Applied Mechanics, Kyoto Japan, Sectional Lecture "Plasticity: Inelastic Flow of Heterogeneous Solids at Finite Strains and Rotations, August 25-31, 1996

14th Army Symposium on Solid Mechanics, Myrtle Beach, SC, Lecture presented "Fracturing in Anisotropic Brittle Solids: Theory and Some Preliminary Experimental Results", October 15-17, 1996.

IMECE'1997, Atlanta, GA, Lectures Presented "Role of Interface Phases on Failure of Silicon Nitride" and "Crack Bridging in In-Situ Toughened Ceramics", November 17 -22, 1996.

9th International Conference on Fracture, Sydney Australia, Invited Keynote Lecture "Tensile Fracturing in Dynamic Compression", April 1-5, 1997.

UCSD IMM Workshop on Multi-Scale Modeling of Polycrystal Plasticity, La Jolla, CA , Lecture on "Dislocation-Based Models of Flow Stress of BCC and FCC Metals with Application to Tantalum and Copper", April 10-11, 1997.

IMECE'97, Northwestern Univ., IL, Organized IMM Sponsored Panel on The Future of Research Organization in the US: Universities, Government Laboratories, and Industry Partnerships. Panel consisted of Drs. J. Achenbach - Center for Quality Engineering and Failure Prevention, NU; B. Frost - Argonne National Laboratory; and O. Richmond - Alcoa Technology Center.

IUTAM Symposium on Micro- and Macro-Structure Aspects of Thermoplasticity, Ruhr-Universitat, Bochum, Germany, August 25, 1997, "Experimentally Based Micromechanical Modeling of Metal Plasticity with Homogenization from Micro - Macro-scale Properties", *Keynote Lecture.*

2nd Euroconference and International Symposium on Materials Instabilities, University of Thessaloniki, Greece, September 1, 1997, "High-Strain-Rate Localization in Metals: Microstructural Characterization, Experimental Observations and Computational Modeling," *Invited Lecture.*

Technical University of Denmark, Denmark, September 6, 1997, "Physically-Based Metal Plasticity: Rate and Temperature Effects," *Invited Lecture.*

ARO Workshop on Mechanics of Heterogeneous Structures, Research Triangle Park, NC March 10-12, 1998, "Physically-Based Computational Modeling of Heterogeneous/Anisotropic Material Systems,"

University of Nebraska, May 29, 1998, "Dislocation Barriers and Plastic Flow of Metals: Experimental Observation and Computation".

12th ASCE EMD Conference, La Jolla, CA, June 17-20, 1998, "From Microscale to Continuum Modeling of Frictional Particulates," "Strain Localization in Particulate Media," "Computational Modeling and Experimental Plasticity," "Bridged Interface Cracks in Isotropic Bi-Materials".

13th National Congress of Applied Mechanics, University of Florida, Gainesville, June 21-26, 1998, "Computational Modeling and Experimental Plasticity," "A Micromechanical Model for the Frictional Flow of Particulate Media". *Invited Lecture*

NSF-IMM Symposium on Micromechanical Modeling for Industrial Materials, University of Washington, Seattle, July 20-22, 1998, "Multi-Inclusion Method for Finite Deformations: Exact Results and Applications," *Keynote Lecture.*

ASME/JSME Pressure Vessel and Piping Conference, San Diego, CA, July 26-30, 1998, "Dynamic Fracture toughness of a 2219-T87 Pressurized Cylindrical Vessel," "Dynamic Fracture Toughness of Miniature Samples Using a New Recovery Hopkinson Technique".

National Materials Advisory Board – Guest Dinner Speaker, Sept. 98 "Recent Developments in Mechanics of Advanced Materials". *Invited Lecture*

IMECE'98, Anaheim, CA, November 1998, "Localized Failure in Dynamic Biaxially Loaded Composite". *Invited Lecture*

IMECE'98, Anaheim, CA, November 1998, Presentation by Jacob Rome (graduate student researcher) "Concrete Deformation under High Strain Rates: Experimental Methods and Results," Symposium on Material Models for Large Deformations.

South Dakota School of Mines and Technology, December 1998, "Recent Developments in Mechanics of Advanced Materials". *Invited Lecture.*

Tuskegee University, Tuskegee, AL, February, 1999, "High-Strain-Rate High-Temperature Response of Materials". *Invited Lecture.*

Arizona State University, February, 1999, "Improvable Bounds on Overall Properties of Heterogeneous Finite Solids."*Invited Lecture*

1999 TMS Annual Meeting, San Diego, CA, March, 1999, "Dynamic Behavior of SiC under Uniaxial Compression". *Invited Lecture*

15th US Army Symposium on Solid Mechanics, Myrle Beach, SC, "On Multi-Scale Homogenization and Average Field Theories".

Mechanics of Heterogeneous Materials Symposium, Grenoble, France, June 1999, "Anistropy in Deformation of Granular Materials". *Invited Lecture*

ASME Joint AMD/MD Conference, Virginia Polytechnique Institute and State University, June 1999, "Tri-Axial Dynamic Compression Experiments Using a Novel Hopkinson Technique," "Strain Localization in Frictional Granules," and "High-Temperature, High-Strain-Rate Receovery Techniques Based on Kolsky's Split Hopkinson Bar Invention".

5.2 Consultative and Advisory Functions to Other Agencies, Laboratories and Universities

4th IMM Young Investigators Meeting on Critical Issues in Materials and Mechanics, Boeing CO, Seattle, WA, Panelist for "Materials Science in Mechanics of Metals: Length Scale and Heterogeneities", July 22-August 2, 1996.

AFOSR Shock Physics Meeting - EAFB, October 18, 1996.

UCSD IMM Workshop on Identification of Basic Research Issues Arising from Industrial uses of Polymeric Structural Materials, Santa Barbara, CA - Panelist Participant, January 12-13, 1997.

AFOSR Grantee/Contractor Conference, Lansdowne, VA , February 2-5, 1997.

13th Ceramic Modeling Working Group Meeting, APG, MD, Organized through Institute for Advanced Technology (Austin TX), Lecture on "Confined Ceramic/W-Penetrator Interaction: Microstructural Observation and Modeling", April 24-25, 1997.

Joint DOE/DOD/NASA Pressure Safety Workshop, Lawrence Livermore National Lab, December 3, 1997.

AFOSR Tyndall & Eglin AFB Grantee Meeting - TAFB, January 17-19, 1998.

Workshop on an NSF Initiative on Long Term Durability of Materials and Structures: Modeling and Accelerated Techniques, University of California, San Diego, February 3, 1998.

ARO Workshop on Mechanics of Heterogeneous Structures, Research Triangle Park, NC March 10-12, 1998.

IMM Workshop on Materials for the Infrastructure, La Jolla, CA, April 1-3, 1998.

ATP Blue Ribbon Panel on Fracture Mechanics, "Fracture Mechanics Models for Airborne Laser's Lethality Program, Kirkland, AFB, April 1998.

Tuskegee University Short Course and Laboratory Instruction, June 10-11, 1999. Short Course entitled "Dynamic Experimentation".

ATP Blue Ribbon Panel on Fracture Mechanics, "Fracture Mechanics Models for Airborne Laser's Lethality Program, Kirkland, AFB, September, 1999.

6. PROFESSIONAL HONORS, AWARDS AND FELLOWSHIPS RECEIVED DURING GRANT PERIOD

Sia Nemat-Nasser -

Recipient of John Dove Isaacs Chair in Natural Philosophy 1995-2000

President of the American Academy of Mechanics, 1996-97

V/Chair of the ASME Materials Division, 1996-97

Technical University of Crete - Gold Medal, 1997

Chair of the ASME Materials Division, 1997-98

Status of Research Effort

1.0 Summary

In the past years, we have designed new experimental techniques to conduct a wide range of experiments, developed a new micromechanics based model, characterized the material under study, and implemented the model using Mathematica with the data we have collected from the experiments and characterization.

Hopkinson bars and a 20 KIPS Instron load frame have been used to conduct experiments, on the concrete and its constituent materials, at high and low strain rates under unixial and triaxial compression. Ultrasonics have been used for non-destructive evaluation (NDE) of the materials. Material characterization has been done using both scanning electron microscopy (SEM), and standard optical tools. A physically based model has been developed, which is based on principle of micromechanics and incorporates damage parameters. A representative volume element (RVE) is the basis of the model. In this approach, a RVE is selected so it contains the important material features that exist in the material. The response is then found for the RVE based on the properties of each constituent, and the entire structure is assumed to have the same response. In the RVE for one proposed model, the mortar, the aggregates, the interfacial transition zone (ITZ) and cracks are included. The dynamic effect and the history are both included via the crack growth. This model is implemented using the commercial software Mathematica.

2.0 Materials

The G-mix concrete (and its constituent materials) for these experiments were generously supplied by Tyndall Air Force Base in Florida. Concrete samples with diameters of two- and three-inches were used. In addition, Tyndall AFB also supplied mortar samples without the largest aggregate, and samples of the limestone used as the large aggregate in the G-mix concrete. Figure 2.1 and Figure 2.2, show examples of the concrete, mortar and limestone samples.

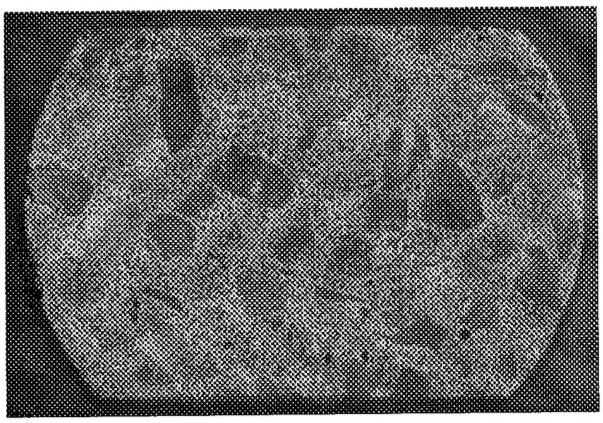

Figure 2.1: Cut-away view of a concrete sample with a 3" diameter

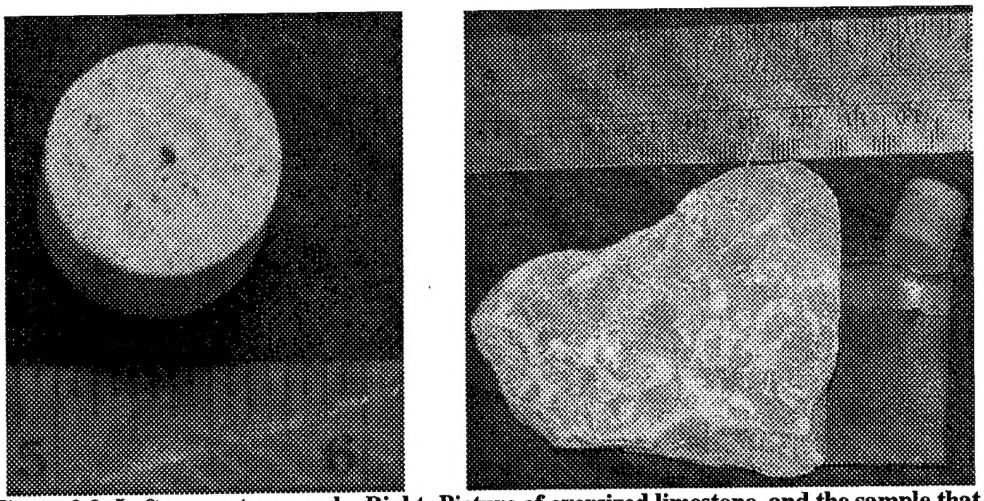

Figure 2.2: Left: a mortar sample. Right: Picture of oversized limestone, and the sample that was machined from it.

3.0 Modeling

The model we have developed is based upon the principles of Micromechanics. A Micromechanics based model examines the physical structure of a material to construct a useful representative volume element (RVE). The proposed model incorporates the main features of the concrete. As shown in Figure 3.1, the limestone aggregate (also referred to as rock) is embedded inside the mortar. The modulus of each material is noted. The mortar itself is inside of an infinitely extended material that has the modulus, **C**, of the overall structure (the concrete). As the material is subject to loading, the cracks will grow according to a dynamic crack growth model. By tracking the length of the cracks within the model and relating that to the strain, the response of the structure is found, and the total damage to the material can be assessed. The different lengths of the cracks will reveal any induced anisotropy.

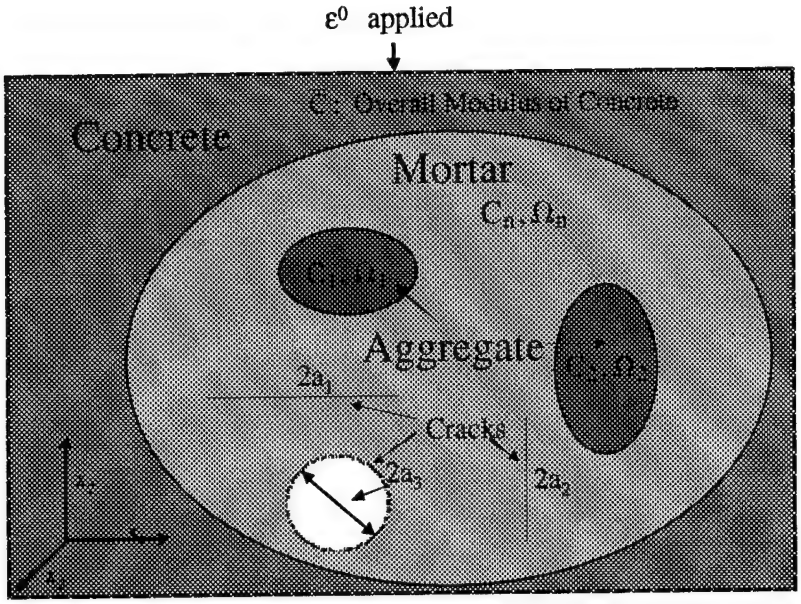

Figure 3.1: Sample RVE of concrete. In this case, two ellipsoidal limestone aggregates and three penny-shaped cracks are contained within the mortar. The mortar is contained within the as-yet unknown average properties of the overall material (the concrete).

Three penny-shaped cracks, each parallel to a different plane, are shown in the above example. Elliptical or winged cracks could also be considered. As the material is loaded, the cracks lengthen according to a dynamic crack-growth law.

The modulus of the mortar and limestone have been measured directly using ultrasonics and during low strain rate loading, and the volume fraction of limestone has been found using optical techniques. In some cases, the effect of the interfacial transition zone (ITZ) may be included via adjustment of the limestone modulus. The number and shape of limestone inclusions in the model can be chosen based upon the size and density of the limestone aggregates in the concrete. In the simplest case, one spherical inclusion is used. In any case, the inclusions must be elliposidal to satisfy the assumptions in the model. Likewise, the mortar inclusion (embedded within the overall material) must be ellipsoidal, and is chosen as spherical for now. The volume of the inclusions is chosen such that the volume fraction is consistent with that found during the material characterization. The inital size and density of the cracks are based upon optical and experimental evaluation.

3.1 Eigenstrains

To explain the model, a few key theories are reviewed [Nemat-Nasser, 1999, Eshelby]. The concept of eigenstrains was enabled by work done by Eshelby. An inclusion is embedded in a homogenous domain (the matrix), which is subject to strains ε^0. If no inclusion were present, then the stresses would be:

$$\sigma^0 = \mathbf{C}:\varepsilon^0, \tag{3.1}$$

where **C** is the elastic modulus. However, the presence of the inclusion causes a disturbance strain, $\varepsilon^d(x)$, throughout the material. The new strains could written as:

$$\varepsilon(x)=\varepsilon^0+\varepsilon^d(x). \tag{3.2}$$

The stresses in the material become:

$$\sigma(x)=\mathbf{C}:\varepsilon(x)=\mathbf{C}:(\varepsilon^0+\varepsilon^d(x)) \text{ in the matrix material} \tag{3.3}$$

$$\sigma(x)=\mathbf{C}^{\Omega}:\varepsilon(x)=\mathbf{C}^{\Omega}:(\varepsilon^0+\varepsilon^d(x))=\sigma^0+\sigma^d(x) \text{ in the inclusion} \tag{3.4}$$

In order to simplify the problem, an equivalent homogenous solid can be considered. Here, the solid is considered to have only one modulus, **C**, which is the modulus of matrix material. In order for this material to have the proper stresses in the inclusion area, eigenstrains, ε^*, are introduced in the inclusion region:

$$\sigma(x)=\mathbf{C}:(\varepsilon(x)-\varepsilon^*(x))=\mathbf{C}:(\varepsilon^0+\varepsilon^d(x)-\varepsilon^*(x))=\sigma^0+\sigma^d(x) \text{ in the inclusion region} \tag{3.5}$$

To provide a consistent solution, it is clear that $\sigma(x)$ from equations (3.4) and (3.5) must be equivalent, therefore:

$$\sigma^0+\sigma^d(x)=\mathbf{C}:(\varepsilon^0+\varepsilon^d(x)-\varepsilon^*(x)) \tag{3.6}$$

The disturbance strains can then be written as:

$$\varepsilon^d(x)=\mathbf{S}(x;\varepsilon^*(x)) \tag{3.7}$$

where **S** is Eshelby's tensor.

Eshelby showed that when the matrix material extends infinitely and is linearly elastic, and the inclusion is an ellipsoid, the eigenstrains, ε^*, are constant in the inclusion, and **S** (Eshelby's Tensor) is a function only of the geometry of the matrix material and the elastic parameters of the matrix. When the matrix is isotropic, it depends only on the geometry and the Poisson ratio. This result, constant eigenstrains and the Eshelby Tensor, will be exploited in the development of this new model.

3.2 Double inclusion method

The double inclusion method is a scheme that is designed to find the modulus for set of materials and geometries [Tanaka; Nemat-Nasser, 1999]. It differs from methods, such as the dilute distribution or self-consistent methods, by better describing the interaction between an inclusion and the surrounding material.The dilute distribution embeds in inclusion within the matrix material, and thus ignores interaction effects. The self-consistent method embeds the inclusion in a material with the as-yet unknown modulus of the overall structure. This accounts for the interaction between inclusions in a limited sense.

The double inclusion method differs. In the simplest case, one ellipsoidal inclusion with modulus $\mathbf{C}^{\Omega}$ is embedded within an ellipsoidal portion of the matrix material, $\mathbf{C}^{\mathbf{M}}$. This outer ellipsoid is contained within an unbounded solid with elasticity $\mathbf{C}$. See Figure 3.2. In the general case, the disturbance strains caused by the inclusion are not constant. However, the average eigenstrains can be found using Eshelby's results [Tanaka]. Using this result, and assuming piecewise constant eigenstrains (e.g., ε^{*1} in the matrix, ε^{*2} in the inclusion), the overall modulus can be estimated.

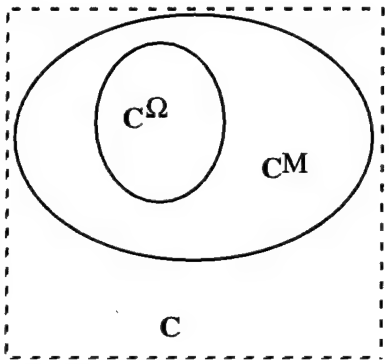

Figure 3.2: Basic schematic of double inclusion method

3.3 Description of the model

An initial estimate of the modulus for the RVE without cracks is made first. The average strain is equal to the applied strain, ε^0. This is also equal to the strain without cracks, ε^{NC}, by definition. The average strain in each element is then:

$$\varepsilon_\alpha = \varepsilon^{NC} + \varepsilon_\alpha{}^{d} \tag{3.8}$$

where $\varepsilon_\alpha{}^{d}$ is the disturbance strain in each element, by definition the difference between the average overall strain and the average strain in each element. The disturbance strains in the α-element are calculated from the eigenstrains in the α-element, plus a volume weighted average of the other eigenstrains. In this case, each element is homogenized by the overall modulus; that is, each element is taken to have the overall modulus and eigenstrains are introduced to keep the stresses consistent.Using that assumption, the average strains and stresses are found for each element. The modulus is defined as the relation between the average stress and the average strain for the entire RVE. These equations are solved iteratively to reach a solution. The mathematical details are shown in Table 3.1.

The model for the RVE which includes cracks follows the same form. The cracks in this case increase the strain in each element, but make no contribution the stress. The additional strain caused by the cracks is found by calculating the crack opening displacement (COD) for each crack. The average stress in each element is found during each iteration while solving the problem. These average stresses are assumed to be farfield stresses, and the COD (and therefore the strain) are found directly. Using a method similar to that used for the non-cracked RVE, the aver-

age stresses and strains in the RVE are found, and the overall modulus is calculated. The equations are solved iteratively to find the solution.

The growth of the cracks is based upon a dynamic crack-growth model. In simple terms, a crack tip experience a crack intensity factor K_I. When K_I reaches some critical crack intensity, K_{IC}, the crack will extend. So it is necessary to find both K_I, likely using linear elastic fracture mechanics as a basis, and K_{IC}, which will take into account the fracture properties of concrete and include a dynamic component. K_I is a function of the material properties and geometry, as well as the general loading condition, and is found using principles of linear elastic fracture mechanics (LEFM). While the limestone and mortar inclusions must be ellipsoidal, the cracks can be any geometry--penny shaped, ellipsoidal, or wing cracks are all possible.

The concrete will eventually fail. In order to best predict the failure, the size of the cracks are tracked and this information is used to help predict the failure. The sample will fail when K_{IC} remains less than K_I. By tracking the crack the crack length, the current damaged state of the material can be assessed.

Since the different cracks will grow at different rates, an anisotropy may develop in the concrete. Even before any loading has taken place, the properties in compression are far different than the properties in tension. The induced anisotropy and the difference between compressive and tensile response are both addressed.

In order for this work to be useful, it must be able to be discretized for use in numerical simulations, such as FEM programs. For that reason, the mathematical complexity in the final model should be manageable. Of course, the most important feature of the model will be its ability to accurately predict the response and failure of the concrete. The model is a physically based, rate dependent, damage model that can be used in simulations to accurately predict the response and failure of concrete. The calculation of modulus for the cracked and non-cracked RVE have been found using Mathematica, and the code is included.

Table 3.1: Mathematical summary of model

Quantity	Non-cracked RVE	Cracked RVE
Applied Strain	ε^0	ε^0
Overall Modulus	C^{NC}	$\overline{C}$
Nominal Stress	$\sigma^0 \equiv C^{NC} : \varepsilon^{NC}$	$\sigma^0 \equiv \overline{C} : \varepsilon^0$
Non-crack strain	$\varepsilon^{NC} = \varepsilon^0$	$\varepsilon^{NC} \equiv D^{NC} : \sigma^0 = D^{NC} : \overline{C} : \varepsilon^0$
Strain in α	$\varepsilon_\alpha = \varepsilon^{NC} + \varepsilon_\alpha{}^{d}$	$\varepsilon_\alpha = \varepsilon^{NC} + \varepsilon_\alpha{}^{d} + \varepsilon_\alpha{}^{crack}$
Average Disturbance strain	$\varepsilon_\alpha{}^{d} = S_\alpha : \varepsilon_\alpha{}^{*} + (S_V - S_\alpha) : \left\{ \sum_{\beta \neq \alpha}^{n} \frac{f_\beta}{1 - f_\alpha} \varepsilon_\beta{}^{*} \right\}$	
	$\varepsilon_n{}^{d} = S_V : \varepsilon_n{}^{*} + \sum_{\alpha=1}^{n-1} \frac{f_\alpha}{f_n (1 - f_\alpha)} (S_V - S_\alpha) : \left\{ \varepsilon_\alpha{}^{*} - \sum_{\beta=1}^{n} f_\beta \varepsilon_\beta{}^{*} \right\}$	
Definitions	S_α : Eshelby Tensor of α inclusion $(\alpha \neq n)$, S_V : Eshelby Tensor of outer ellipsoid f_α : Volume fraction of α, $\varepsilon_\alpha{}^{*}$: Average eigenstrain in α	
Crack strain	N/A	$\varepsilon_\alpha{}^{crack} = H_\alpha' : \sigma_\alpha = H_\alpha' : C_\alpha : \left(1^{(4s)} + B_\alpha\right) : D^{NC} : \sigma^0 = H_\alpha : \sigma^0$
Definitions	$H_\alpha \equiv H_\alpha' : C_\alpha : \left(1^{(4s)} + B_\alpha\right) : D^{NC}$, $B_\alpha : \varepsilon^{NC} \equiv \varepsilon_\alpha{}^{d}$ H_α' : Crack relation for Dilute distribution model	
Stress in α	$\sigma_\alpha = C_\alpha : \varepsilon_\alpha = C_\alpha : \left(\varepsilon^{NC} + \varepsilon_\alpha{}^{d}\right)$	$\sigma_\alpha = C_\alpha : \left(\varepsilon_\alpha - \varepsilon_\alpha{}^{crack}\right) = C_\alpha : \left(\varepsilon^{NC} + \varepsilon_\alpha{}^{d}\right)$ $= C_\alpha : \left(1^{(4s)} + B_\alpha\right) : \varepsilon^{NC} = C_\alpha : \left(1^{(4s)} + B_\alpha\right) : D^{NC} : \sigma^0$
Consistency	$C_\alpha : (\varepsilon_\alpha) = C^{NC} : (\varepsilon_\alpha - \varepsilon_\alpha{}^{*})$	$C_\alpha : \left(\varepsilon_\alpha - \varepsilon_\alpha{}^{crack}\right) = \overline{C} : (\varepsilon_\alpha - \varepsilon_\alpha{}^{*})$
	$C_\alpha : \left(\varepsilon^{NC} + \varepsilon_\alpha{}^{d}\right) = C^{NC} : \left(\varepsilon^{NC} + \varepsilon_\alpha{}^{d} - \varepsilon_\alpha{}^{*}\right)$	$C_\alpha : \left(\varepsilon^{NC} + \varepsilon_\alpha{}^{d}\right) = \overline{C} : \left(\varepsilon^{NC} + \varepsilon_\alpha{}^{d} + \varepsilon_\alpha{}^{crack} - \varepsilon_\alpha{}^{*}\right)$
Average strain	$< \varepsilon >= \varepsilon^{NC} + < \varepsilon^{d} >= \left(1^{(4s)} + S_V : A\right) : \varepsilon^{NC}$	$< \varepsilon >= \varepsilon^{NC} + < \varepsilon^{d} > + < \varepsilon_\alpha{}^{crack} >$ $= \left(1^{(4s)} + S_V : A + < H > : C^{NC}\right) : \varepsilon^{NC}$
Definitions	$A : \varepsilon_{NC} \equiv < \varepsilon^{*} >$: Definition of concentration tensor, A, $< \varepsilon^{d} >= S_V : < \varepsilon^{*} >$, Mori – Tanaka Volume average $< (\cdot) > \equiv \sum_{\alpha=1}^{n} f_\alpha (\cdot)_\alpha$	
Average stress	$< \sigma >= \sum_{\alpha=1}^{n} f_\alpha C_\alpha : \left(\varepsilon_{NC} + \varepsilon_\alpha{}^{d}\right)$ $= \sum_{\alpha=1}^{n} f_\alpha C^{NC} : \left(\varepsilon_{NC} + \varepsilon_\alpha{}^{d} - \varepsilon_\alpha{}^{*}\right)$ $= C^{NC} : \left(\varepsilon_{NC} + < \varepsilon^{d} > - < \varepsilon^{*} >\right)$ $= C^{NC} : \left(1^{(4s)} + \left(S_V - 1^{(4s)}\right) : A\right) : \varepsilon_{NC}$	$< \sigma >= \sum_{\alpha=1}^{n} f_\alpha C_\alpha : \left(\varepsilon_{NC} + \varepsilon_\alpha{}^{d}\right)$ $= \sum_{\alpha=1}^{n} f_\alpha \overline{C} : \left(\varepsilon_{NC} + \varepsilon_\alpha{}^{d} - \varepsilon_\alpha{}^{*} + \varepsilon_\alpha{}^{crack}\right)$ $= \overline{C} : \left(\varepsilon_{NC} + < \varepsilon^{d} > - < \varepsilon^{*} > + < \varepsilon_\alpha{}^{crack} >\right)$ $= \overline{C} : \left(1^{(4s)} + \left(S_V - 1^{(4s)}\right) : A + < H > : C^{NC}\right) : \varepsilon_{NC}$
Definition of Modulus	$C^{NC} : < \varepsilon > \equiv < \sigma >$	$\overline{C} : < \varepsilon > \equiv < \sigma >$
Modulus	Non-cracked: $C^{NC} = C^{NC} : \left(1^{(4s)} + \left(S_V - 1^{(4s)}\right) : A\right) : \left(1^{(4s)} + S_V : A\right)^{-1}$	
	Cracked: $\overline{C} = \overline{C} : \left(1^{(4s)} + \left(S_V - 1^{(4s)}\right) : A + < H > : C^{NC}\right) : \left(1^{(4s)} + S_V : A + < H > : C^{NC}\right)^{-1}$	

4.0 Experiments

4.1 Hopkinson Bar Tests on Concrete

A 3-inch Hopkinson bar is used to test the concrete at high strain rates. The incident and transmitted bars are each 8-feet long. All the bars are made out of 1040 steel, and elastic wave speed is 202,500 inches/ second. This steel has a lower hardness than the maraging steel that Hopkinson Bars are generally made from. This led to the probability of the bars being damaged. To prevent any damage, one-inch thick 1040 steel platens are placed between the sample and the bars.

A six foot brake bar was used to stop the momentum and dissipate the energy from the tests. Two clamps are secured around the brake bar, and the friction between the clamp and the brake bar is used to stop its momentum. The brake is what stops the momentum of the Hopkinson Bar and dissipates its energy. The brake works by clamping a three inch diameter bar (the brake bar) that is coaxial with and next to the transmitted bar. The friction between the clamp and the brake bar dissipates the energy in the system as the brake bar slides through the clamp. A torque wrench is used to tighten the clamp the desired amount. A photograph and a schematic of the Hopkinson bar are shown in Figure 4.1.

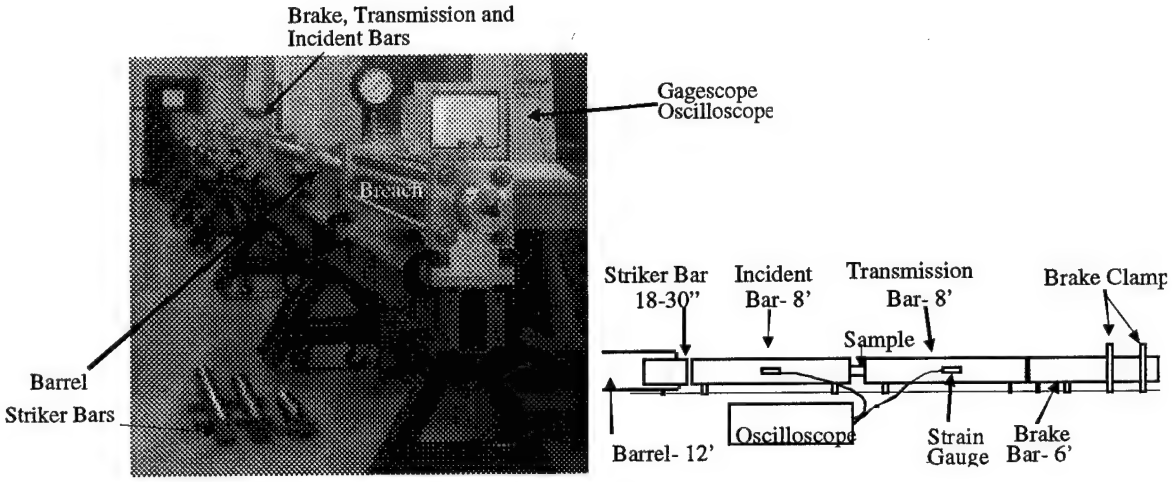

Figure 4.1: Photograph and schematic of 3-inch Hopkinson Bar

Acquisition equipment

For the Hopkinson Bar tests, similar acquisition equipment was used. The strain gauges were from Micromeasurements of Raleigh, North Carolina, and were attached using Loctite Depend adhesive. Two gauges are located on every incident and transmitted bar, and are used in a Wheatstone Bridge to measure the strain, using 30V non-switching DC power supplies from Kepco.

The digital oscilloscope used to capture the data is a computer controlled Gagescope. The Gagescope is a pair of hardware cards that are installed in a PC. This equipment is able to sample either two channels of data at up to 100MHz or 4 channels at up to 50MHz, using a 12-bit digitizer.For the present work, samples rates around 2MHz are used. The Gagescope is controlled by software that runs under MS-DOS.

Loading Profiles

For the Hopkinson Bar experiments, the elastic wave profile affects the material response. In order to maintain a constant strain rate during an experiment, a squarish wave profile is needed. If the rise time is too quick, the sample may not come into equilibrium, and the test results may be suspect. An elastic wave with a slower rise time is more likely to result in establishing equilibrium during a test, but a constant strain rate cannot be maintained. Figure 4.2 shows two examples of what the incident pulse and strain rates typically were during experiments. In the rest of this paper, these two classes will be broadly referred to as square and triangular pulses.

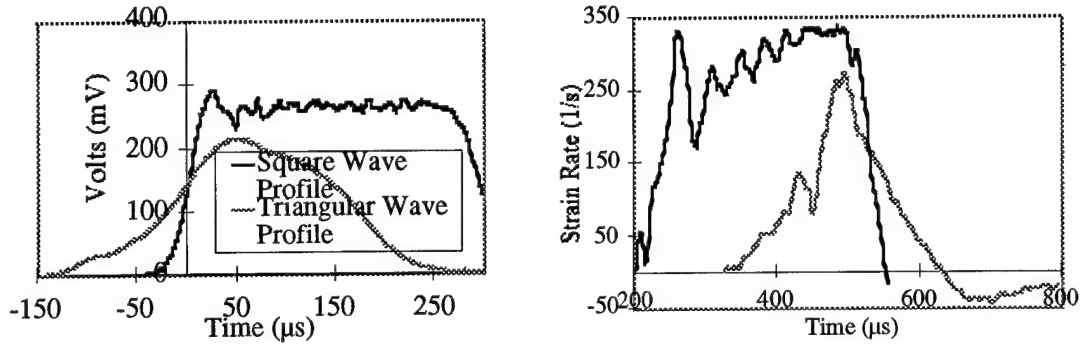

Figure 4.2: Typical elastic wave (incident pulse) profiles and strain rates used in testing

The square waves are normally generated during the striker bar- incident bar impact. In order to create a triangular pulse, a damping material must be used. For these experiments, commercially pure aluminum was used to aid in the generation of the triangular pulse. This material was chosen due to its uniformity, and its low rate of strain-hardening. It was important to choose a material which had little strain hardening; otherwise the incident and striker bars could be damaged.

Uniaxial tests

Typical unixial samples are shown in Figure 4.3. The samples were all 3" in diameter, and ranged in length from 0.75" to 2.25". During the tests, the samples were held in place between two 1" thick platens with tape. The platens were secured using the rings seen below.

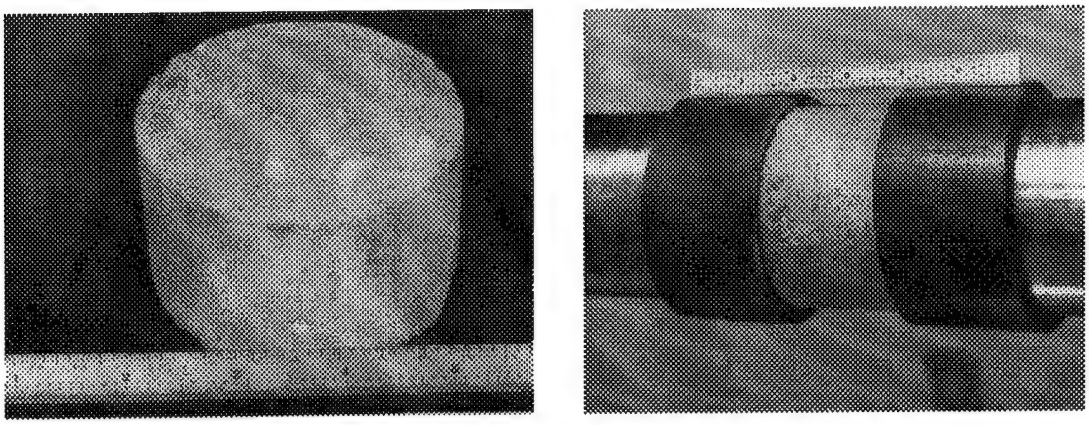

Figure 4.3: Typical samples used in unconfined concrete tests.

Tests were conducted using both triangular and square wave profiles at a number of strain rates. The strain rate effect can be seen in Figure 4.4. The samples in this tests were each 1" long, and were destroyed after the test by the reloading of the sample. The strain rates reported below roughly correspond to the peak strain rates, and the results for the triangular and square wave profiles cannot be directly compared. However, it is observed that the samples with the triangular wave profile have a smoother measured response.

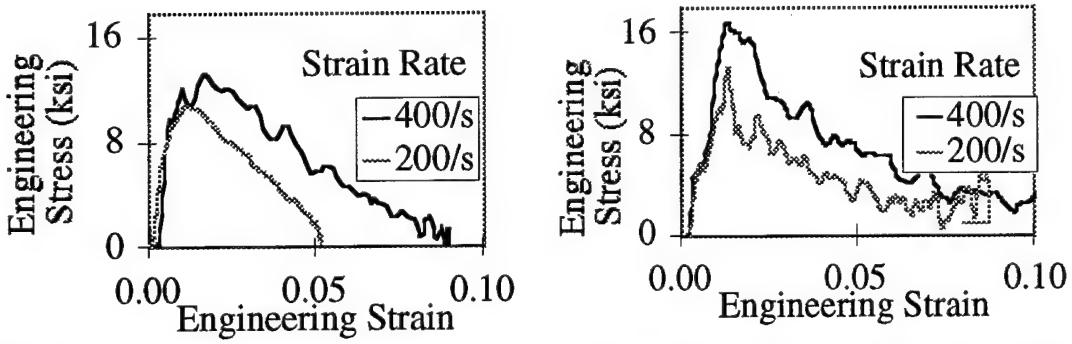

Figure 4.4: Strain rate effect on unconfined concrete using triangular (left) and square loading profiles

Uniaxial tests with high speed photography

High speed photographs were taken during some experiments. Some samples were photographed without cutting parallels, as shown in Figure 4.3. Other samples had parallel surfaces cut across the diameter of the sample, similar to what is shown in Figure 4.12. Photographs of the tests are shown in Figure 4.5 to Figure 4.8, where the loading is horizontal.The strain rate at failure was about 250/s. Half of the results presented show an entire face, and the others focus on a smaller section of the sample. A Hadland Imacon 792 was used. This camera uses one 3" x 5" piece of Polaroid film, and 8 images were taken. These images can be taken at rates from of 50 thousand to 20 million frames per second. The resolution is 10 lines/mm, which results in an image size of about 200 x 200 pixels. For these tests, the frame rate used was 50,000/s (20μs).

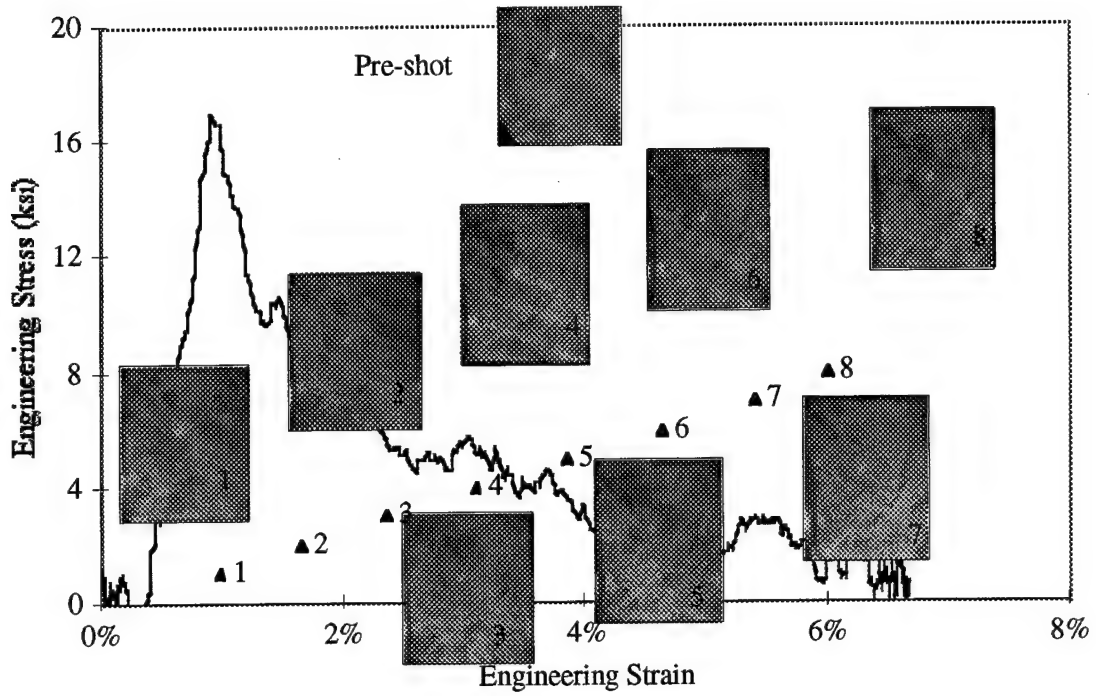

Figure 4.5: High speed photographs of cut-away section of concrete. Here, the entire surface is shown

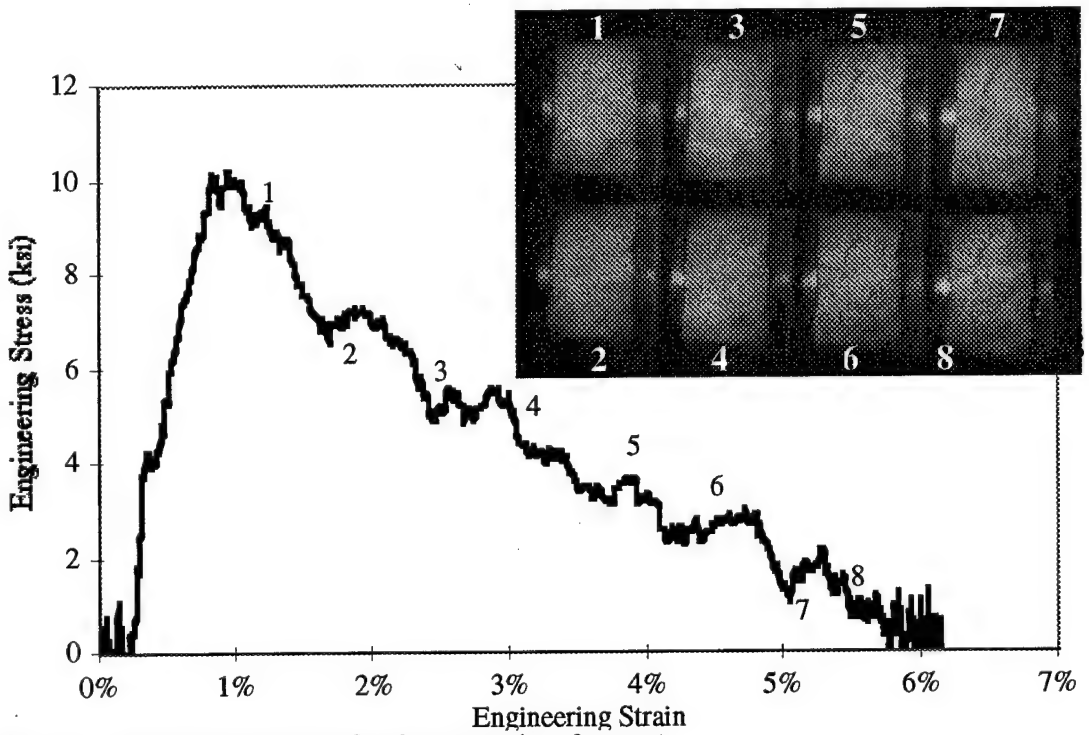

Figure 4.6: High speed photographs of uncut section of concrete

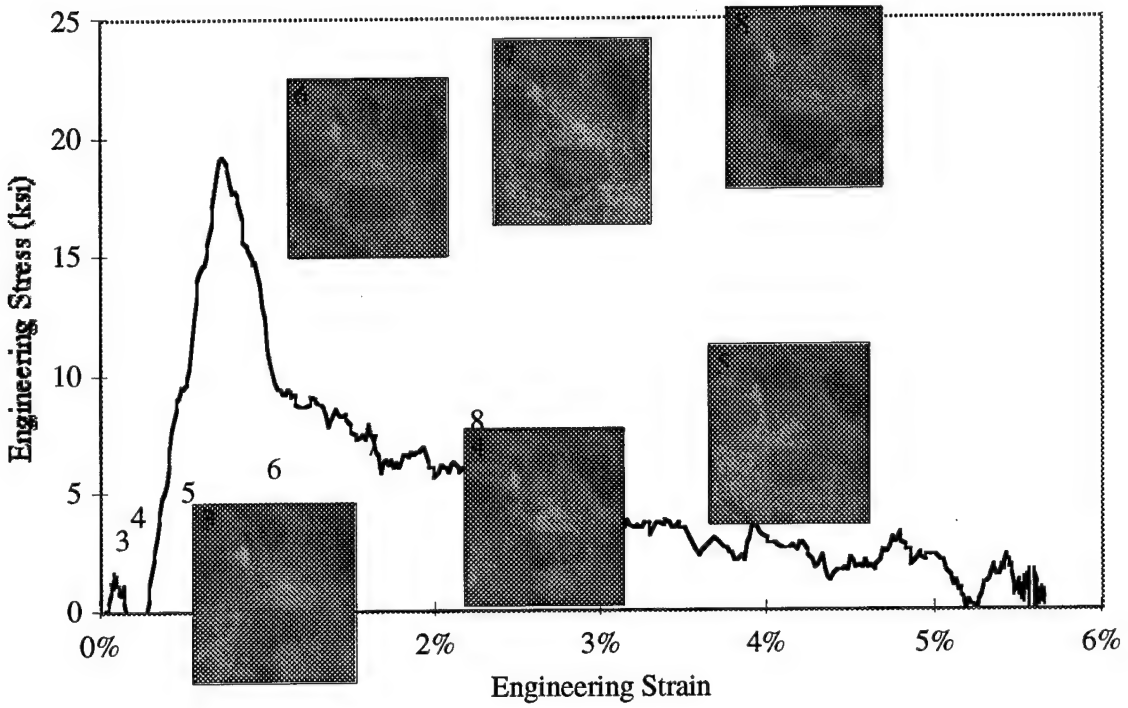

Figure 4.7: High speed photographs showing a close-up of a cut-away section

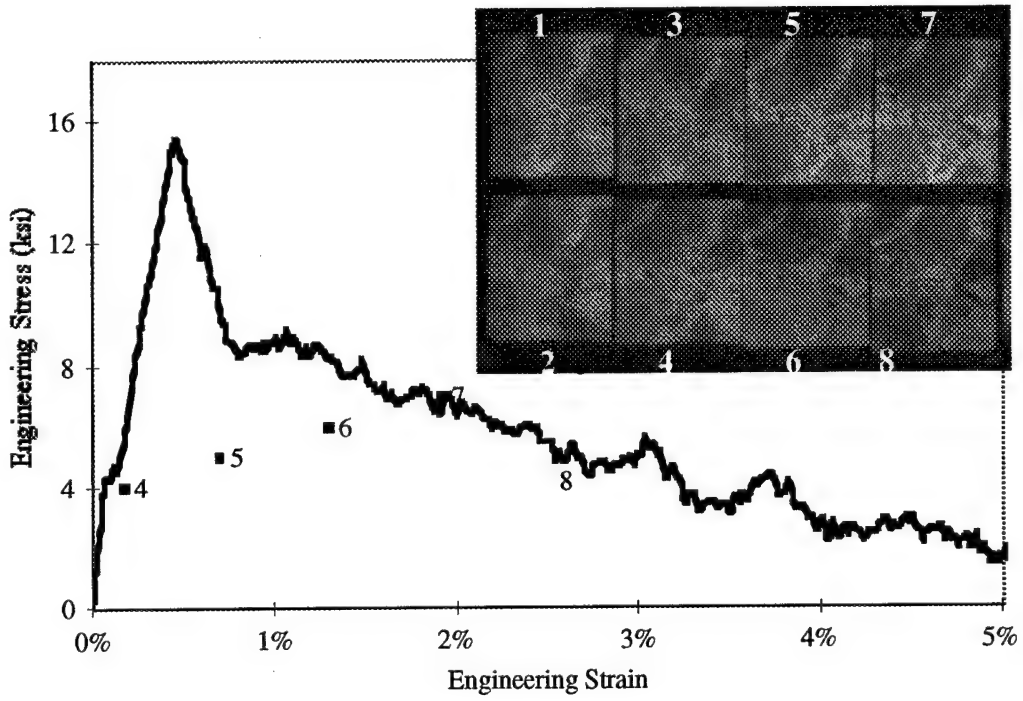

Figure 4.8: More high speed photographs showing a close-up of a cut-away section

Cracks can be seen growing axially and radially in Figure 4.5. In this test, one crack became dominant as it grew the quickest across the sample. The large crack grew across the mortar, but other cracks are observed which split some limestone aggregates.

Figure 4.6 shows lots of crack formation after the peak stress has been reached. Some cracks at this stage are growing parallel with the loading axis, but the most active cracks are perpendicular to the initial loading direction

In Figure 4.7 a crack can clearly be seen propagating at the sharp tip of a limestone aggregate. Under careful observation, a crack can be seen growing from the tip of a limestone piece in Figure 4.8. These pictures illustrate a crack growing across the sample from right to left. In all cases, significantly more crack growth was observed after the failure stress. However, the resolution of the camera, as well as the total number of frames, limited what could be observed.

Triaxial tests

Stainless steel T-bolt band clamps (similar in shape to, but stronger than, hose clamps) provided the radial confinement for some triaxial tests. The clamps have a thickness of 0.025", and are each 0.75" wide. The clamps are wrapped around the samples and loaded to a specified confining pressure. A thin sheet of Teflon is located between the clamp and the sample to reduce friction in the axial direction. On some samples, platens were clamped along with the concrete; on the other samples the platens were taped to the clamps. In all cases, the plastic tubes held the platens (and samples) in place. A torque wrench was used to load the samples.

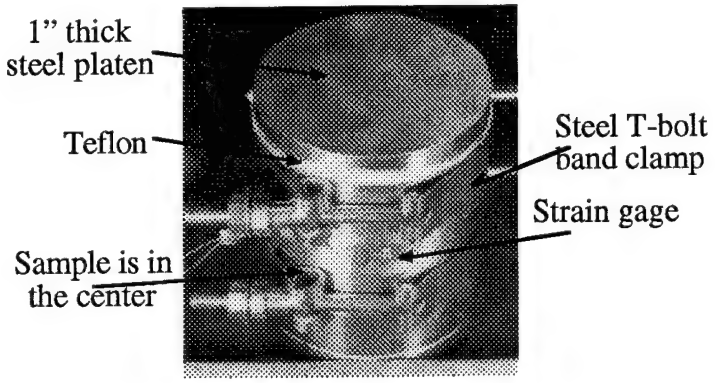

Figure 4.9: Typical confined-clamp sample

On a number of samples, the relation between the applied torque and the radial confinement was calibrated; the hoop strain in the clamp was measured using a strain gage. The radial stress and is calculated using that measurement. On one sample, the hoop strain in the clamp was measured dynamically. In this case, the radial and volumetric strain in the sample were calculate.

As shown in Figure 4.10, the steel band clamp clearly yielded possibly before and certainly during the test. This suggests that after an initial rise in the confining pressure, it increases much more slowly. Thus an initial difference in confining pressure is unlikely to produce different results.This test was done at a nominal strain rate of 200/s with a triangular wave.

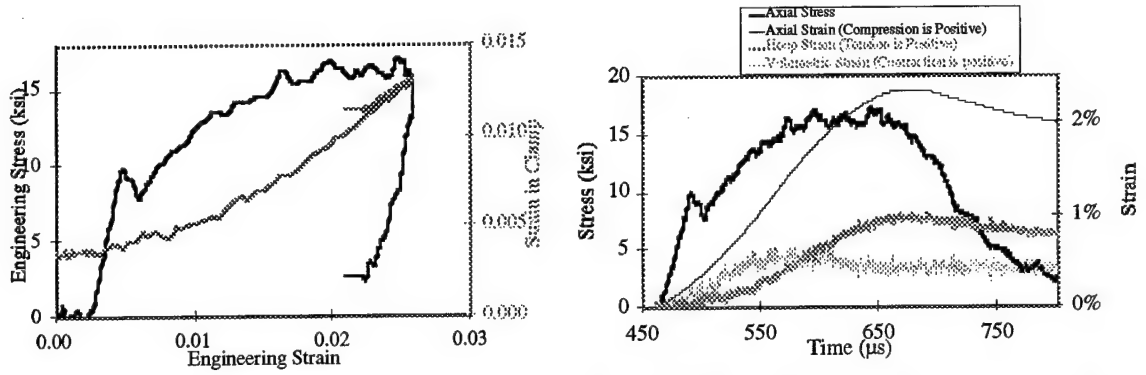

Figure 4.10: Dynamic measurement of hoop and volumetric strain. The figure on the left shows that the steel clamp yielded during the experiment; the figure on the right calculates the concrete response during the test.

As shown in Figure 4.11, the two samples were initially subject to different confining pressures. However, the response of the two samples are nearly identical, due to the increase in confinement during the test. The samples, each 1.5" long, were tested at a strain rate of about 200/s, with a triangular elastic wave profile.

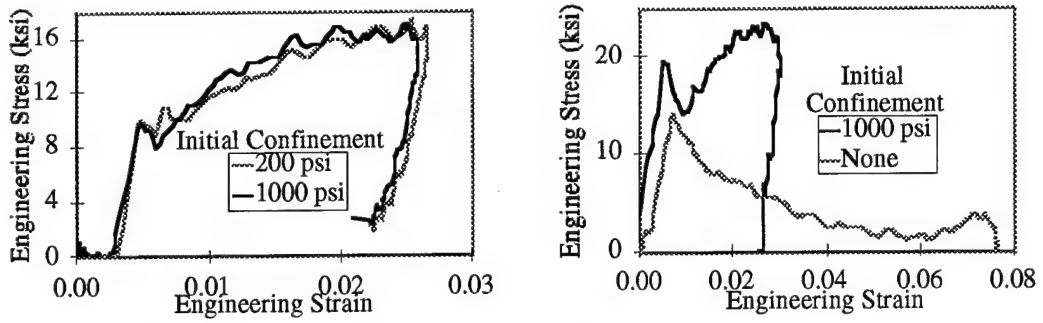

Figure 4.11: Effect of initial confinement on concrete response and response of radially confined and unconfined concrete.

The presence or absence of confinement has a dramatic effect on the material response and failure. Figure 4.11 shows an example for a pair of 2 inch long specimens which have been tested at a strain rate of 200/s using a square loading profile. After testing, confined samples appeared largely undamaged while the unconfined samples have been shattered. One reason the unconfined samples were turned into rubble is because they were subject to repeated loading by the Hopkinson Bar. Micrographs taken of the confined samples after testing are presented in the next section.

Microscopy on damaged samples

Most of the samples tested with the clamp confinement remained largely intact after the experiments. Some of these samples were used for microscopy, and the micrographs are presented here. The cross section, one inch thick, that was examined is shown in Figure 4.12. Both top and bottom were cut with a diamond saw, and one face was polished.

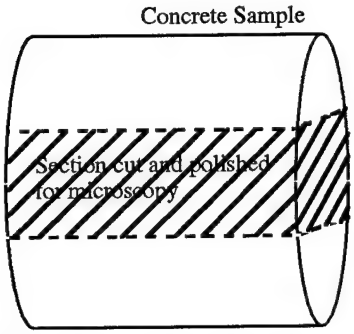

Figure 4.12: Cross section used for microscopy

The first pictures were taken of a sample that had been loaded with a triangular loading profile at a peak strain rate of 200/s, under 200psi initial confinement, sample cnc3-2q-4. The arrows show the direction of the axial straining. An axial crack through a rock is plainly visible in Figure 4.13. Sample cnc3-2q-2 was 2.25" long and loaded with a trapezoidal pulse at a strain rate of 100/s with an initial confinement of 1000psi. The sample was tested a total of 3 times. The two photographs, Figure 4.14, focus on what appears to be a crack running part of the way through a rock in the sample. Most of the rocks did not have visible cracks in the axial direction.

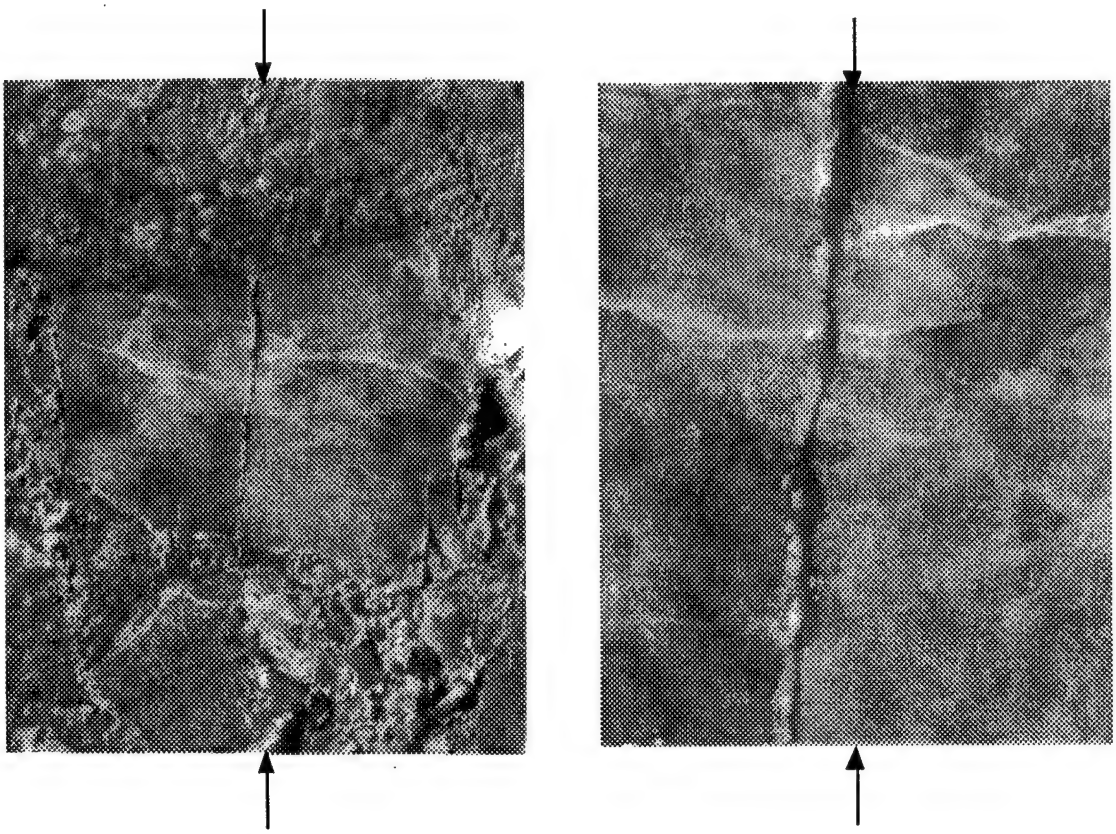

Figure 4.13: Axial crack in sample cnc3-2q-4, at 5x (left) and 20x (right)

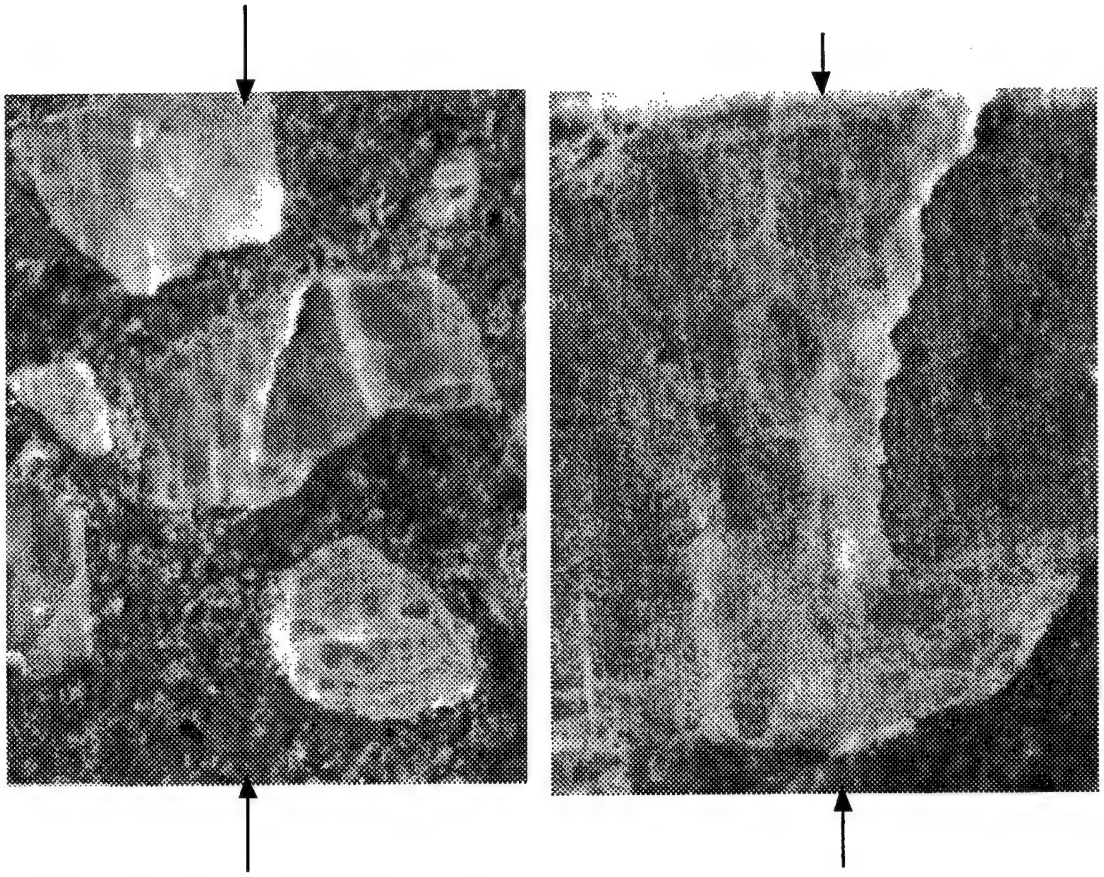

Figure 4.14: Crack in cnc3-2q-2, 5x (left) and 20x (right)

Pneumatic Pressure Vessel

A large diameter pressure vessel provides the pneumatic confinement; see Figures 3 and 4. A steel cylinder of 6 inches outside diameter and half-inch wall thickness surrounds the sample. The aluminum end plates are each 1 inch thick, and are held together by four 3/8 inch bolts. A rubber sleeve, secured by hose clamps, is placed over the sample to prevent direct contact between the sample are the high-pressure gas. O-rings are used to seal the pressurized chamber. A band clamp and the brake bar restrain the incident and transmission bars, respectively, to prevent them from moving apart. This pressure vessel provides a constant radial confinement of up to 1000 psi.

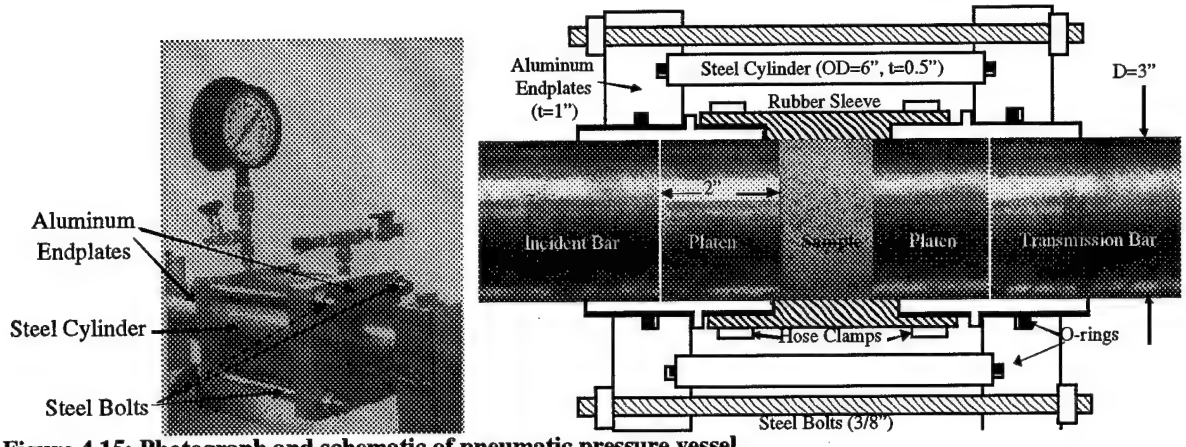

Figure 4.15: Photograph and schematic of pneumatic pressure vessel

4.2 Experiments on rock and mortar

In addition to testing the concrete, the constituent materials have also been tested. Ultrasonics have been used for NDE, an Instron machine has been used for low strain rate uniaxial testing, and Hopkinson bars have been used for uniaxial and triaxial tests at high strain rates.

Low strain rate tests on mortar

Mortar samples prepared without the limestone aggregate have been tested. Three samples, each about 0.75" long and 0.7" in diameter, were tested at low strain rates. A 20kips hydraulic Instron machine is used for running low strain rate experiments. National Instruments hardware and software (Labview) were used for the data acquisition. Data was sampled at rates from 1/s to 10/s. In the tests, the load measurement is very accurate. However, the strain measurement is not as accurate. In both cases, the strain measurement is largely dependent on how well the strain gage or extensometer is attached to the sample. The attachment of the strain gage to the mortar is good at low strains, but at higher strains the deformation may be affected locally by the strain gage and the glue used to attach it. At low strains, Young's Modulus is found to be 4.7×10^6 psi. One result is shown in Figure 4.16.

High strain rate uniaxial tests on mortar

Uniaxial tests were done on the mortar samples using the 3/4" recovery Hopkinson bar. The 3/4" Hopkinson bar is used to test the rock and mortar at high strain rates. This Hopkinson Bar is made from Maraging steel, and the elastic wave velocity was measured as 200,000 in/s. The incident and transmitted bars are each 48" long, and striker bars between 3 and 18 inches may be used with this tool. The bar is designed to prevent reloading of the sample, and the use of the recovery Hopkinson bar allows for valid post-experiment assessment of samples. This assessment includes NDE with ultrasonics, or ultimate strength tests using low strain rate testing equipment. As shown in Figure 4.16, the small difference in strain rates had little effect on the response, but more tests are needed to verify this. On the right, the response of the mortar at high and low strain rates is contrasted. It is obvious that the failure stress is much higher at the high strain rates.

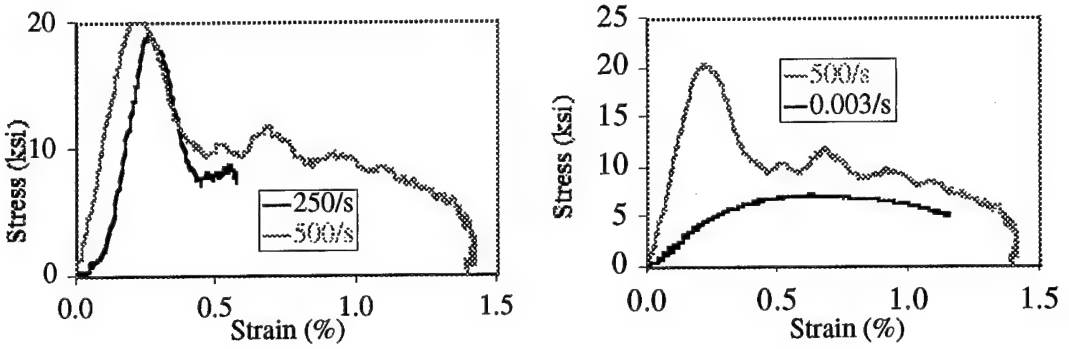

Figure 4.16: Rate effects on mortar response

High strain rate triaxial tests on mortar

The classical Hopkinson Bar can be modified to allow dynamic triaxial compressive loading of a sample. This technique simultaneously loads the sample in the axial and radial directions. Figure 4.17 and Figure 4.18 are a photograph and schematic of this system. The striker (A) impacts the first incident bar (B), generating the incident pulse. The wave is transmitted to the second incident bar (C) and the incident tube (F). (Note: With this design, the reflected pulse can not be measured directly, so it is calculated as the difference between the transmitted pulse and the incident pulse.) The sample (D) is inside a Teflon tube (G), which in turn is inside an aluminum sleeve (H).

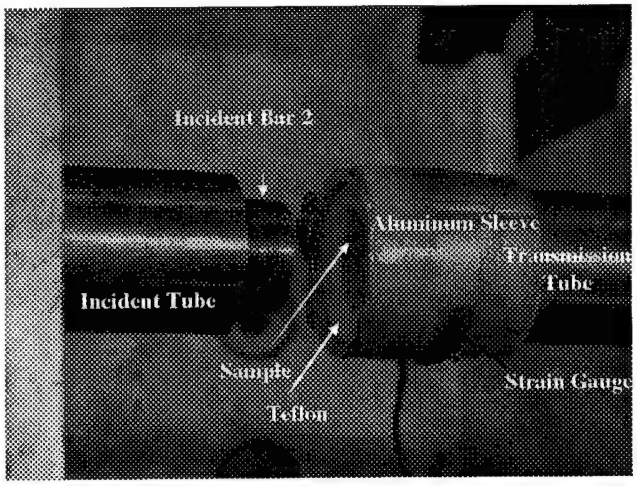

Figure 4.17: Photograph of triaxial load cell

The confinement is provided by the Teflon, which is dynamically compressed between the incident tube (F) and the transmission tube (I). Restrained laterally by the aluminum sleeve, a large hydrostatic stress is produced in the Teflon. This pressure creates a large radial stress on the sample. The hoop strain in the aluminum sleeve is measured, and the radial confining stress is calculated. The radial stress can be controlled independently from the axial stress and strain to a limited extent, by, e.g., altering the thickness of the aluminum sleeve to control when the sleeve yields.

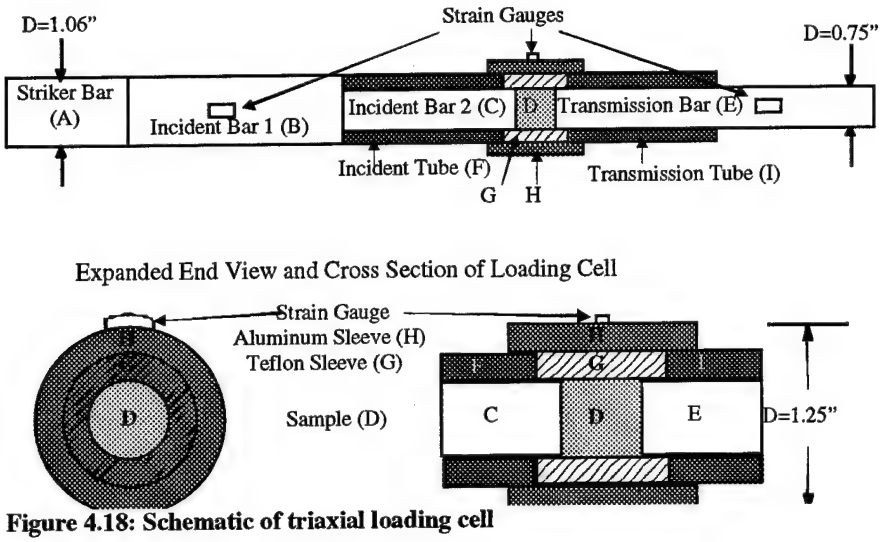

Figure 4.18: Schematic of triaxial loading cell

The simultaneous loading in the radial and axial directions is assured by the design of the bar-- the stress waves in the incident bar and incident tube are generated at the same time, they are made of the same material, and they have nearly the same length. Thus, the stress wave in the incident bar reaches the sample (loading it axially) at the same time as the stress wave in the incident tube reaches the Teflon (loading the sample radially).

This method has been used to test several samples. The confinement had a tremendous effect on the response of the mortar. Figure 4.19 shows the response during three tests. Samples TXMK and TXML were tested under identical conditions, except TXML used the thinner aluminum sleeve. During that test, the sleeve yielded, which resulted in a lower confining pressure, which is estimated in that figure. The lower radial stress led to lower axial stresses. Comparison with Figure 4.16 shows the dramatic effect confinement has on the mortar response.

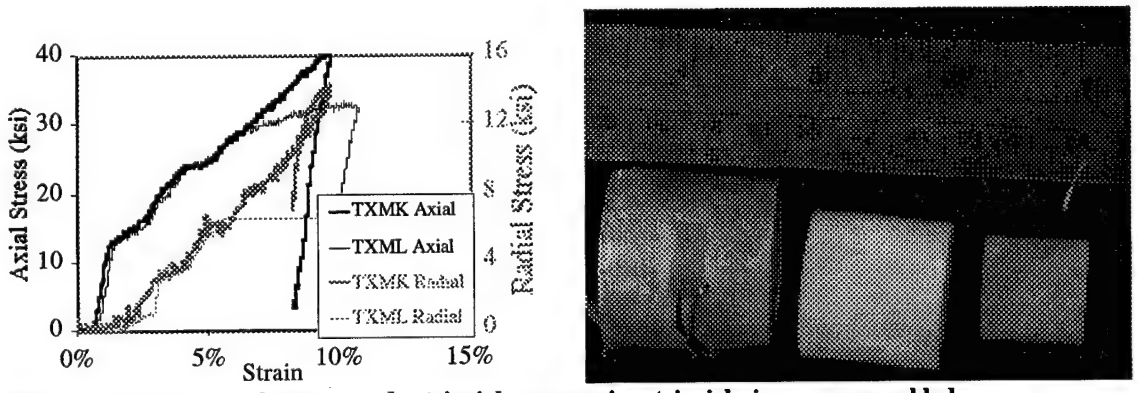

Figure 4.19: Response of mortar under triaxial compression, triaxial pieces un-assembled.

A scanning electron microscope (SEM) has been used to observe some of the tested an untested samples. Figure 4.20 shows a micrograph of an untested concrete sample and a tested mortar sam-

ple. Many more cracks are observed in the tested samples than the untested samples, when observed under similar magnifications.

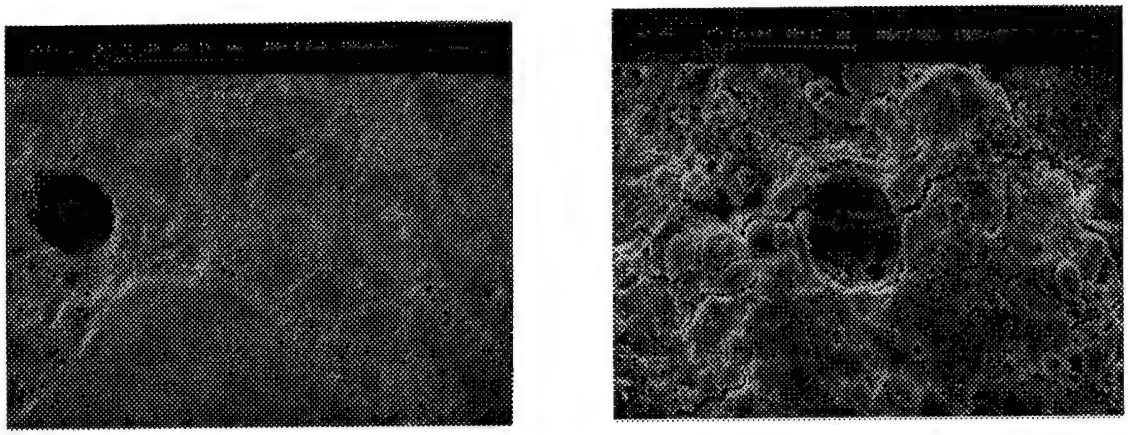

Figure 4.20: SEM micrographs of: untested concrete (25x); mortar tested in triaxial compression (500x)

Low strain rate tests on limestone

Low strain rate tests were done using the 20 kips Instron machine. The samples were 0.5" in diameter and 0.5" long. The data shows that the rocks fail elastically under uniaxial compression. As is the case with the mortar, the load measurement is very accurate. The displacement measurement should be more accurate than it is for the mortar, because the strain gages adhere much better to the surface of the limestone than they do to the mortar.The measured modulus for the rock is about 10.5 x 10^6 psi. See Figure 4.21.

High strain rate uniaxial tests on limestone

The 3/4" Hopkinson bar, was used to conduct uniaxial tests on the limestone. The use of the recovery Hopkinson Bar allowed for the retrieval of damaged by intact samples, which are evaluated using NDE.

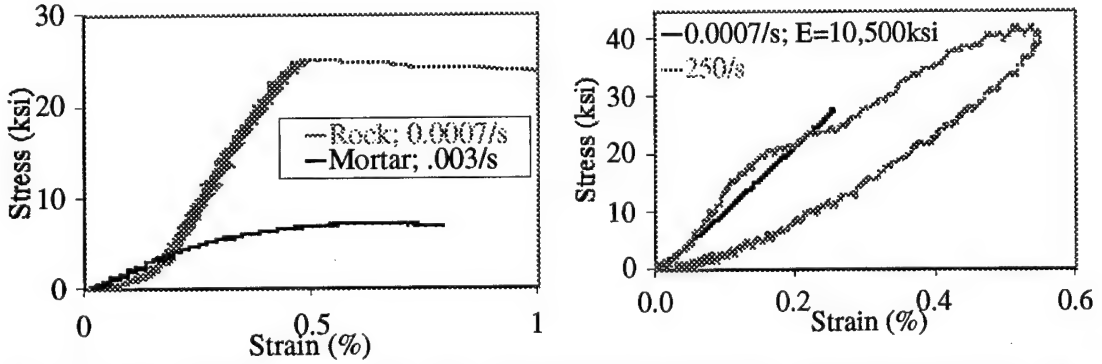

Figure 4.21: Comparison of rock and mortar response (left); high and low strain rate limestone response

Figure 4.21 shows the response of the limestone. Comparison with the results from low strain rate testing show that limestone has a greater failure stress under dynamic conditions. However, due to the variability from sample to sample, no definite conclusion can be drawn at this time, though it is suspected that this is a real effect. Above, Figure 4.22 shows a comparison of the rock and mortar at high strain rates. The limestone clearly has a greater failure stress than the mortar.

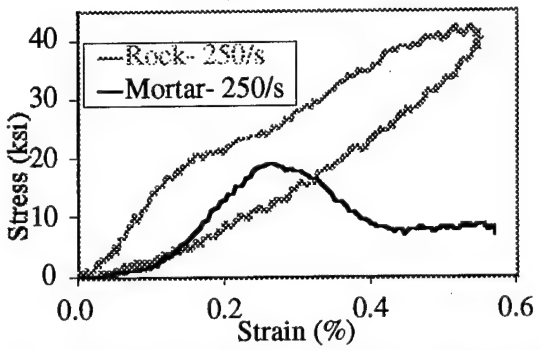

Figure 4.22: Comparison of rock and mortar response at high strain rates

NDE of limestone and mortar using ultrasonics

Ultrasonic equipment can be used for NDE of a range of materials. Samples may be evaluated with ultrasonics, tested on a recovery Hopkinson Bar, then tested again with ultrasonics to assess changes. The equipment used in the current study is described briefly below.

The wave generation and initial transmission to the sample is identical to the procedure used by Aashish Rohatgi in his research at UCSD. He describes the set-up, in part, as follows [Rohatgi, pp.42-45]:

> A constant sinusoidal wave (CW) of the desired frequency and amplitude (~125mv) is produced by the Marconi Synthesizer and supplied to the waveform generator in the MBS-8000 ultrasonic measurement system, which in turn generates a high voltage (~100 V) signal (RF) of the same frequency. The pulse width, amplitude and frequency of the RF signal are controlled via a computer interface. The RF pulse excites the broad band transducer which sends a high frequency pulse...

The transducer is put into contact with the sample, using water as a couplant for longitudinal tests, and honey as a couplant for shear test. Another transducer is placed on the opposite end of the sample, which is excited by the acoustic wave and generates a voltage, which is in then measured. Comparison of the initial signal and the transmitted signal allows for computation for the velocity through the sample.

The acquisition equipment is the same digital Gagescope that is described in section . In this case, the Gagescope samples the data at 60MHz.

Transducers with natural resonant frequencies of 5MHz and 10MHz were used. The transducers were supplied by Panametrics. Both shear and longitudinal transducers were used in the experiments, and all contained a piezoelectric crystal.

Measurements of the acoustic wave velocities were done on both the rock and mortar samples, plus maraging steel for comparison. The elastic modulus and the Poisson ratio can be calculated from the plane (C_1) and shear (C_2) wave velocities, when the density is also known.

$$\nu = \frac{C_1^2 - 2 \times C_2^2}{2 \times (C_1^2 - C_2^2)} \tag{4.1}$$

$$E = \frac{C_1^2 \times \rho \times (1+\nu) \times (1-2\nu)}{(1-\nu)} \tag{4.2}$$

Inspection of the calculated elastic constants for steel reveal that the method is valid. The difference between the elastic modulus found via low strain rate testing (4.7 x 10^6 psi) differs significantly from the ultrasonic testing (3.3 x 10^6 psi). The low strain rate testing will be repeated, taking care in the displacement measurement, which can be difficult to make accurately.

Table 4.1: Wave velocities and calculated elastic constants of rock and mortar

Material	Specific Density	Wave Velocities (10^3 in/s)		Poisson Ratio	Young's Modulus (10^6 psi)	Range
		Plane (C_1)	Shear (C_2)			
Rock	2.69	258	134	0.32	11.9	2.5%
Mortar	2.11	131	85	0.15	3.3	1.6%
Maraging Steel	8.06	223	117	0.31	27.2	N/A

The results from the ultrasonic testing are summarized in Table 4.1. One test result is shown in Section 4.23. For the limestone, the two separate calculations of the elastic modulus are quite close, 10.5 x 10^6 psi for the low strain rate testing, and 11.9 x 10^6 psi for the ultrasonic testing. Some of these tests may be repeated to ensure a statistically sound database.

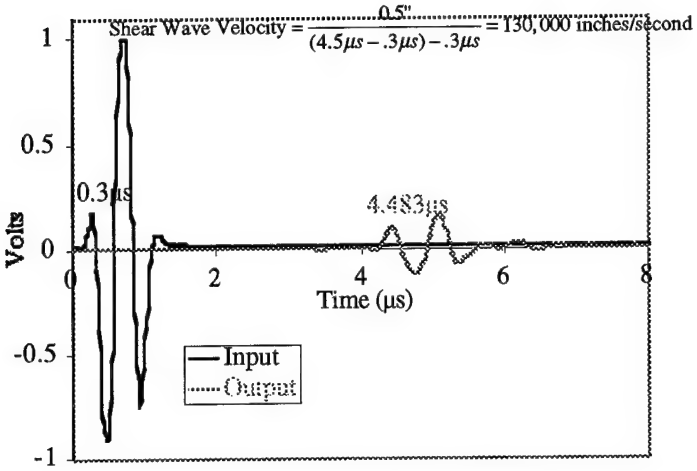

Figure 4.23: Measurement of the shear wave speed in rock using ultrasonics

5.0 Material characterization

Examples have already been shown of optical and SEM micrographs used to aid in the characterization of the sample. Those pictures yield sound information on the size and density of cracks in the materials. To measure the volume fraction of limestone, a direct quantitative method is used. First, a concrete sample is scanned using a computer scanner, Figure 5.1. Then, the limestone aggregates are outlined with the aid of a graphics tablet. The limestone is then set to black, and the software counts the percent of black pixels. In the example shown below, the limestone has a 41% volume fraction. This information is then used to determine the size of the inclusions in the model.

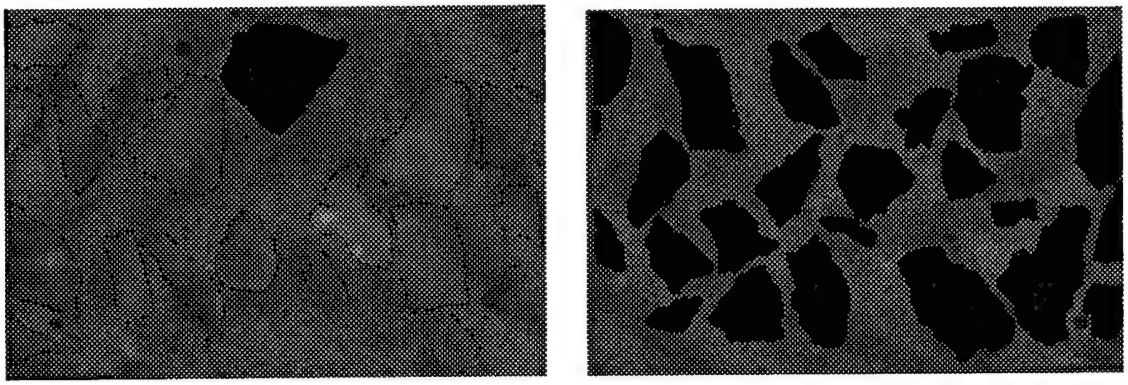

Figure 5.1: Scan of concrete sample with limestone outlined; scan of concrete with limestone darkened.

6.0 Conclusions

A RVE has been designed to embody the primary features of the concrete, based upon its physical microstructure. This model is designed using information from material characterization and experimental results. Using micromechanics, fracture mechanics and damage mechanics, the

response and failure of the concrete is predicted. The modulus is found by numerically implementing the model in Mathematica. The crack growth and sample failure criteria are being added to the current implementation.

7.0 References

Ashby, M., and Sammis, C., "The Damage Mechanics of Brittle Solids in Compression," *PAGEOPH*, Vol. 133, No. 3, (1990) pp. 489-521.

Bancroft, D. "The Velocity of Longitudinal Waves in Cylindrical Bars," *Phys. Rev.* 59, 588-593 (1941).

Eshelby, J.D. (1957), "The Determination of the Elastic Field of an Ellipsoidal Inclusion, and Related Problems", *Proc. R. Soc.* London, Ser. A, Vol. 241, 376-396.

Hopkinson, B., *Phil Trans. R. Soc. Lond. A*, Vol. 213 (1914) 437-456.

Hopkinson, J., *Proc. Manch. Lit. Phil. Soc.*, Vol. 11 (1872) 40.

Hopkinson., B. *Proc. R. Soc. Lond. A*, Vol. 74 (1905) 498.

Kolsky, H (1963)., *Stress Waves in Solids*, Dover, New York.

Kolsky, H., "An Investigation of the Mechanical properties of Materials at Very High Rates of Loading," *Proc. Phys. Soc.*, Vol. 62 (1949) 667.

Lifshitz, J.M and Leber, H.,., "Data Processing in the Split Hopkinson Pressure Bar Tests," *Int. J. Impact Engng*, Vol. 15, No. 6, pp. 723-733, 1994.

Love, A.E.H., *Mathematical Theory of Elasticity* (Cambridge University Press, 1927).

Mehta, P., and Monteiro, P., *Concrete*, Prentice Hall, New Jersey, 1993.

Mori, T., and Tanaka, K., "Average Stress in Matrix and Average Elastic Energy of Materials with Misfitting Inclusions," *Acta. Met.*, Vol. 21, 571-574 (1973).

Nemat-Nasser, S., and M. Hori (1999), *Micromechanics: Overall Properties of Heterogeneous Materials*, North-Holland, New York.

Nemat-Nasser, S., and H. Deng, "Strain Rate Effect o Brittle Failure in Compression," *Acta. Metall. Mater.*, Vol. 42, No. 3, pp. 1013-1024, 1994.

Nemat-Nasser, S., J.B. Isaacs, and J.E. Starrett, "Hopkinson Techniques for Dynamic Recovery Experiments," *Proc. Roy. Soc.*, Vol. 435A, (1991) 371-391.

Nemat-Nasser, S., N. Yu, and M. Hori, "Solids with Periodically Distributed Microcracks," *Int. J. Solids Structures*, Vol.30, No. 15, pp. 2071-2095, 1993.

Nemat-Nasser, S., Yu, N., and Hori, M. (1993), "Bounds and estimates of overall moduli of composites with periodic microstructure", *Mechanics of Materials*, 15, 3, pp.163-181.

Nemati, K., P. Monteiro, and K. Scrivener, "Analysis of Compressive Stress-Induced Cracks in Concrete," *ACI Materials Journal*, Vol. 95, No. 5, pp. 617-630, 1998.

Nemati, K., P. Monteiro, and N. Cook, "A New Method or Studying Stress-Induced Microcracks in Concrete," *Journal of Materials in Civil Engineering*, Vol. 10, No. 3, (1998) pp. 128-134.

Nemati, K., "Fracture Analysis of Concrete Using Scanning Electron Microscopy," *Scanning*, Vol. 19, pp. 426-430, 1997.

Pochhammer, L., J.f. Math. (Crelle) 81, 324 (1876).

Rohatgi, A., "A Microstructural Investigation of Shock Loading Effects in FCC Materials," ph.d. Thesis, University of California, San Diego, 1999.

Ross, C., P. Thompson, and J. Tedesco, "Split Hopkinson Pressure-Bar Tests on Concrete and Mortar in Tension and Compression," *ACI Materials Journa*l, V. 86, No. 5, (1989) pp. 475-481.

(* Set-up problem *)

(* Physical parameters *)

```
Clear["Global`*"]; (* clears all variables from memory *)
n = 2; (* Number of micro-elements *)
ν_ref = 1/3; μ_ref = 1; (* Initial properties of body *)
K_ref = 2 μ_ref (1 + ν_ref) / (3 (1 - 2 ν_ref)); (* Initial Bulk Modulus of Body *)

μ_1 = 50; ν_1 = 1/3; μ_2 = 1; ν_2 = 1/3; (* Properties of micro-elements *)

Youngs_2 = 2 μ_2 (1 + ν_2); (* Young's modulus of mortar *)

fcrack_1 = 0; fcrack_2 = 0; fcrack_3 = .1;

f_1 = .4;  f_2 = 1 - f_1; (* Volume percent of micro-elements *)

ncIterations = 10;

Iterations = 25; (* Number of loops to iterate over *)

weight_notn = 0;

weight_n = (1 - (1 - f_n) weight_notn) / f_n;

Print[{weight_n, weight_notn}];
```

(* Define basic functions used to create and transform elasticity and Eshelby Tensors *)

```
(* The
  W matrix needed to convert the compliance tensor to a matrix, and its inverse. *)

W = Table[0, {i1, 6}, {i2, 6}];

Do[W[[i, i]] = 1, {i, 3}];

Do[W[[i, i]] = 2, {i, 4, 6}];
```

```
InvW = Inverse[W];

(* Set up size and initial values for some vectors and matrices *)

Zero6 = Table[0, {i, 6}]; (* Length 6 vector with a magnitude=0 *)

Zero6by6 = Table[0, {i1, 6}, {i2, 6}];

A = Zero6by6; Aprime = Zero6by6; Aprimenew = Zero6by6;

Acrack = Zero6by6;

distrain1 = Zero6by6;

distrain2 = Zero6by6;

Do[εigen_β = Table[x_β_i, {i, 6}], {β, n}]; (* Fills out eigenstrain vectors *)

(* Widgets to populate and transform elasticity and eshelby tensors *)

first[1] = 1; first[2] = 2; first[3] = 3; first[4] = 2; first[5] = 3; first[6] = 1;

second[1] = 1; second[2] = 2; second[3] = 3; second[4] = 3; second[5] = 1; second[6] = 2;

MakeTwo[Mod4_] :=
 Module[{DumMod2}, DumMod2 = Table[0, {i1, 6}, {i2, 6}]; Do[DumMod2[[i, j]] =
    Mod4[[first[i], second[i], first[j], second[j]]], {i, 6}, {j, 6}]; Return[DumMod2];];


PopEshSphere[νDum_] :=
 Module[{DumMod}, DumMod = Table[0, {i1, 3}, {i2, 3}, {i3, 3}, {i4, 3}];
  Do[DumMod[[i, j, i, j]] = (4 - 5 νDum)/(15 (1 - νDum)), {i, 3}, {j, 3}];
  Do[DumMod[[i, j, j, i]] = (4 - 5 νDum)/(15 (1 - νDum)), {i, 3}, {j, 3}];
  Do[DumMod[[i, i, j, j]] = (5 νDum - 1)/(15 (1 - νDum)), {i, 3}, {j, 3}];
  Do[DumMod[[i, i, i, i]] = ((5 νDum - 1)/(15 (1 - νDum)) + 2 (4 - 5 νDum)/(15 (1 - νDum))), {i, 3}]; Return[DumMod];];


PopIsoMod[μDum_, νDum_] :=
 Module[{DumMod}, DumMod = Table[0, {i1, 3}, {i2, 3}, {i3, 3}, {i4, 3}];
```

```
Do[DumMod[[i, j, i, j]] = μDum, {i, 3}, {j, 3}];
Do[DumMod[[i, j, j, i]] = μDum, {i, 3}, {j, 3}];
Do[DumMod[[i, i, j, j]] = 2 μDum νDum / (1 - 2 νDum), {i, 3}, {j, 3}];
Do[DumMod[[i, i, i, i]] = 2 μDum (1 - νDum) / (1 - 2 νDum), {i, 3}]; Return[DumMod];];
```

```
perm1[1] = 2; perm1[2] = 3; perm1[3] = 1; perm2[1] = 3; perm2[2] = 1; perm2[3] = 2;
```

```
PennyCrackStress[mod_, νDum_, μDum_, dens1_, dens2_, dens3_] :=
Module[{compliance, compliance2, modcrack},
 compliance = Zero6by6; compliance2 = InvW . Inverse[mod] . InvW;
  compliance[[1, 1]] = 8 (1 - νDum) / (3 μDum) × dens1;
  compliance[[2, 2]] = 8 (1 - νDum) / (3 μDum) × dens2;
  compliance[[3, 3]] = 8 (1 - νDum) / (3 μDum) × dens3;
  compliance[[4, 4]] = 4 (1 - νDum) / (3 (2 - νDum) μDum) × (dens2 + dens3);
  compliance[[5, 5]] = 4 (1 - νDum) / (3 (2 - νDum) μDum) × (dens3 + dens1);
  compliance[[6, 6]] = 4 (1 - νDum) / (3 (2 - νDum) μDum) × (dens1 + dens2);
  compliance2 += compliance;
  modcrack = InvW . Inverse[compliance2] . InvW - mod;
  Return[{compliance, modcrack}];];
```

(* Populate Eshelby and elasticity tensors *)

```
Do[s_α = MakeTwo[PopEshSphere[ν_ref]], {α, n - 1}]; (* Eshelby tensor of micro-elements *)
```

```
s_VV = MakeTwo[PopEshSphere[ν_ref]]; (* Initial Eshelby tensor of outer ellipsoid *)
```

```
Do[c_α = MakeTwo[PopIsoMod[μ_α, ν_α]], {α, n}]; (* Micro-elements *)
```

```
s_V = MakeTwo[PopEshSphere[ν_ref]]; (* Reset Initial Eshelby tensor of outer ellipsoid *)
```

$$\mu_M = \left(\frac{1}{1 + f_1 \frac{1}{\left(\frac{\mu_{ref}}{\mu_{ref} - \mu_1} - 2\, s_V[[4,4]]\right)}} + 1 - f_1 \frac{1}{\left(\frac{\mu_{ref}}{\mu_{ref} - \mu_1} - 2\, s_V[[4,4]]\right)} \right) \Big/ 2;$$

```
(* Initial guess for shear modulus of matrix *)
```

$\mathbf{C}_{ref}$ = MakeTwo[PopIsoMod[μ_M, ν_{ref}]]; (* Initial Reference elasticity *)

```
(* Check for relevance of crack strain *)
```

(* Define functions specific for this problem *)

(* Eigenstrains averaged over non–α elements *)

```
OtherEigenAverage[α_, n2_] := Module[{Result}, Result = Table[0, {i1, 6}, {i2, 6}];
```

$$\text{Result} = \sum_{\beta=1}^{n2} \left(\frac{f_\beta}{1 - f_\alpha} \varepsilon\text{igen}_\beta \right) - \frac{f_\alpha}{1 - f_\alpha} \varepsilon\text{igen}_\alpha ; \text{Return[Result];}];$$

```
(*****************************************************************************)
```

```
Do[{
```

(* Define and evaluate Disturbance strain for all micro–elements *)

```
StrainDisturb[α_, n1_] := Module[{Result}, Result = Table[0, {i1, 6}, {i2, 6}];
    Result = Sα . W . εigenα + (Sv - Sα) . W . OtherEigenAverage[α, n1]; Return[Result];];
  (* defines disturbance strain for all microelements except outer ellipsoid *)
Do[εdistα = StrainDisturb[α, n], {α, n - 1}]; (* Evaluate disturbance strain *)
```

$$\varepsilon\text{dist}_n = \mathbf{S}_V \cdot \mathbf{W} \cdot \varepsilon\text{igen}_n + \sum_{\alpha=1}^{n-1} \frac{f_\alpha}{f_n\,(1 - f_\alpha)} (\mathbf{S}_V - \mathbf{S}_\alpha) \cdot \mathbf{W} \cdot \left(\varepsilon\text{igen}_\alpha - \sum_{\beta=1}^{n} f_\beta \, \varepsilon\text{igen}_\beta \right);$$

```
  (* Find disturbance strain for outer ellipsoid *)

Do[{
```

(* Sets up each case for one non–zero component *)

```
ε = Zero6; (* resets ε to zero *)
εigenew1 = Zero6; εigenew2 = Zero6;
εigenAve = Zero6;
ε[[γ]] = 1/IntegerPart[1 + γ/3.5]; (* Set one component of ε=1 *)
```

(* Solve for eigenstrain for each case *)

```
{{{εigenew1, εigenew2}}} = ReplaceAll[{εigen1, εigen2},
      {Solve[{C1 . W . (ε + εdist1) - Cref . W . (ε + εdist1 - εigen1) == Zero6,
         C2 . W . (ε + εdist2) - Cref . W . (ε + εdist2 - εigen2) == Zero6},
        {(x1)1, (x1)2, (x1)3, (x1)4,
         (x1)5, (x1)6, (x2)1, (x2)2, (x2)3, (x2)4, (x2)5, (x2)6}]}];
```

(* Finds volume-average eigenstrain *)

$$\varepsilon\text{igenAve} = \sum_{\alpha=1}^{n} f_\alpha \, \varepsilon\text{igenew}_\alpha ;$$

```
Do[A[[i, γ]] = εigenAve[[i]], {i, 6}];
}, {γ, 6}];
```

$$\mathbf{C}_{new} = \mathbf{C}_{ref} \cdot \mathbf{W} \cdot (\text{InvW} + (\mathbf{S}_V - \text{InvW}) \cdot \mathbf{W} \cdot \text{A}) \cdot \text{Inverse}[\text{InvW} + \mathbf{S}_V \cdot \mathbf{W} \cdot \mathbf{A}] \cdot \text{InvW};$$

$$\mathbf{C}_{ref} = \mathbf{C}_{new};$$

$$\mu_{new} = \mathbf{C}_{ref}[[4, 4]];$$

$$\nu_{new} = \frac{\mathbf{C}_{ref}[[1, 2]]}{2\,(\mathbf{C}_{ref}[[1, 2]] + \mu_{new})};$$

$$K_{new} = \frac{2\,\mu_{new}\,(1 + \nu_{new})}{3\,(1 - 2\,\nu_{new})};$$

```
Clear[StrainDisturb];
```

$\mathbf{S}_V$ = MakeTwo[PopEshSphere[ν_{new}]]; (* Eshelby tensor of outer ellipsoid *)
Do[$\mathbf{S}_\alpha$ = MakeTwo[PopEshSphere[ν_n]], {α, n - 1}]; (* Eshelby tensor of micro-elements *)

```
      }, {ncIterations}];
(*****************************************************************************)
```

$$\{D_{crack2}, C_{crack}\} = \text{PennyCrackStress}[\mathbf{C}_{ref}, \nu_n, \mu_n, \text{fcrack}_1, \text{fcrack}_2, \text{fcrack}_3];$$

$$C_{nocrack} = \mathbf{C}_{ref};$$

$$D_{nocrack} = \text{InvW} \cdot \mathbf{Inverse}[C_{nocrack}] \cdot \text{InvW};$$

(* Find the concentration tensor *)

(* Large do-loop *)

```
Do[{
```

(* Define and evaluate Disturbance strain for all micro-elements *)

```
StrainDisturb[α_, n1_] := Module[{Result}, Result = Table[0, {i1, 6}, {i2, 6}];
    Result = Sα . W . εigenα + (SV - Sα) . W . OtherEigenAverage[α, n1]; Return[Result];];
  (* defines disturbance strain for all microelements except outer ellipsoid *)
Do[εdistα = StrainDisturb[α, n], {α, n - 1}]; (* Evaluate disturbance strain *)
```

$$\varepsilon\text{dist}_n = \mathbf{S}_V \cdot \mathbf{W} \cdot \varepsilon\text{igen}_n + \sum_{\alpha=1}^{n-1} \frac{f_\alpha}{f_n\,(1 - f_\alpha)}\,(\mathbf{S}_V - \mathbf{S}_\alpha) \cdot \mathbf{W} \cdot \left(\varepsilon\text{igen}_\alpha - \sum_{\beta=1}^{n} f_\beta\,\varepsilon\text{igen}_\beta\right);$$

```
  (* Find disturbance strain for outer ellipsoid *)
Do[{
```

(* Sets up each case for one non-zero component *)

```
ε = Zero6; (* resets ε to zero *)
```

$\varepsilon\text{igenew}_1$ = Zero6; $\varepsilon\text{igenew}_2$ = Zero6; $\varepsilon\text{distnew}_1$ = Zero6; $\varepsilon\text{distnew}_2$ = Zero6;

```
εigenAve = Zero6;
ε[[γ]] = 1 / IntegerPart[1 + γ/3.5]; (* Set one component of ε=1 *)
D_crack = D_crack2 . W . C_2 . W . (InvW + Aprimenew) . W . D_nocrack ;
    εcrackref = D_crack . W . C_nocrack . W . ε;
    εcrack_n = weight_n × εcrackref;
Do[εcrack_α = weight_notn × εcrackref, {α, n - 1}];

(* Solve for eigenstrain for each case *)
{{{εigenew_1, εigenew_2, εdistnew_1, εdistnew_2}}} =
    ReplaceAll[{εigen_1, εigen_2, εdist_1, εdist_2},
     {Solve[{C_1 . W . (ε + εdist_1) - C_ref . W . (ε + εcrack_1 + εdist_1 - εigen_1) == Zero6,
        C_2 . W . (ε + εdist_2) - C_ref . W . (ε + εcrack_2 + εdist_2 - εigen_2) == Zero6},
       {(x_1)_1, (x_1)_2, (x_1)_3,
        (x_1)_4, (x_1)_5, (x_1)_6, (x_2)_1, (x_2)_2, (x_2)_3, (x_2)_4, (x_2)_5, (x_2)_6}]}];

(* Finds volume-average eigenstrain *)
εdistfinal_1 = Zero6;
    εdistfinal_2 = Zero6;
(* Junk=ReplaceAll[εdist_1,
      {(x_1)_1→, (x_1)_2, (x_1)_3, (x_1)_4, (x_1)_5, (x_1)_6, (x_2)_1, (x_2)_2, (x_2)_3, (x_2)_4, (x_2)_5, (x_2)_6→}]; *)
εigenAve = Σ_{α=1}^{n} f_α εigenew_α;
Do[A[[i, γ]] = εigenAve[[i]], {i, 6}];
    Do[Aprime[[i, γ]] = εdistnew_2[[i]], {i, 6}];
    Do[distrain1[[i, γ]] = εdistnew_1[[i]], {i, 6}];
    Do[distrain2[[i, γ]] = εdistnew_2[[i]], {i, 6}];

}, {γ, 6}];
(* C_new=C_ref . W . (InvW+(S_V-InvW) . W . A) . Inverse[InvW+S_V . W . A] . InvW; *)
C_new = C_ref . W . (InvW + (S_V - InvW) . W . A + D_crack . W . C_nocrack) .
    Inverse[InvW + S_V . W . A + D_crack . W . C_nocrack] . InvW;
Aprimenew = Aprime;
C_ref = (C_new + Transpose[C_new]) / 2;
  C_ref = C_new ;
μ_new = C_ref[[4, 4]];
ν_new = C_ref[[1, 2]] / (2 (C_ref[[1, 2]] + μ_new));
K_new = 2 μ_new (1 + ν_new) / (3 (1 - 2 ν_new));

Clear[StrainDisturb];

S_V = MakeTwo[PopEshSphere[ν_new]]; (* Eshelby tensor of outer ellipsoid *)
Do[S_α = MakeTwo[PopEshSphere[ν_n]], {α, n - 1}]; (* Eshelby tensor of micro-elements *)

{D_crack2, C_crack} = PennyCrackStress[C_nocrack, ν_n, μ_n, fcrack_1, fcrack_2, fcrack_3];
    }, {Iterations}];

(* Do[
  {C_final = (C_ref . W . (InvW + (S_V - InvW) . W . A) + Acrack) . Inverse[InvW + S_V . W . A + A4] . InvW;
   C_ref = C_final ; μ_new = C_ref[[4, 4]];
   ν_new = C_ref[[1, 2]] / (2 (C_ref[[1, 2]] + μ_new)); S_V = MakeTwo[PopEshSphere[ν_new]]}, {10}]; *)
```

$C_{final} = C_{ref}$;

$C_{final} = (C_{ref} \cdot W \cdot (InvW + (S_V - InvW) \cdot W \cdot A + D_{crack} \cdot W \cdot C_{nocrack}) + 0\, C_{crack}) \cdot$
Inverse[InvW + $S_V \cdot W \cdot A + D_{crack} \cdot W \cdot C_{nocrack}$] · InvW;

$$Mu_{DDE} = 1 - f_1 \frac{1}{\frac{\mu_{ref}}{\mu_{ref} - \mu_1} - 2\, S_{VV}[[4, 4]]};$$

$$Mu_{DDS} = \frac{1}{1 + f_1 \frac{1}{\frac{\mu_{ref}}{\mu_{ref} - \mu_1} - 2\, S_{VV}[[4, 4]]}};$$

$$\text{Print}\left[\text{NumberForm}\left[\left\{\mu_1,\ f_1,\ \nu_{new},\ \frac{K_{new}}{K_{ref}},\ Mu_{DDE},\ \mu_{new},\ Mu_{DDS}\right\}\right]\right];$$

Print[MatrixForm[C_{ref}]];

Print[MatrixForm[$C_{nocrack}$]];

comp = InvW · Inverse[$C_{nocrack}$] · **InvW;**

comp2 = InvW · Inverse[C_{final}] · **InvW;**

Print[MatrixForm[C_{final}]];

$$\text{Print}\left[\left\{C_{final}[[4, 4]],\ \left(1 + \text{fcrack}_3 \frac{16\,(1 - \nu_n)}{3\,(2 - \nu_n)}\right)^{-1}\right\}\right];$$

$$\text{Print}\left[\left\{\text{comp}[[3, 3]] / \text{comp2}[[3, 3]],\ \left(1 + \text{fcrack}_3 \frac{16\,(1 - \nu_n^2)}{3}\right)^{-1}\right\}\right];$$

Print[MatrixForm[comp2]];

Clear[OtherEigenAverage];

Print[MatrixForm[($C_{nocrack}$) · **Inverse[InvW +** D_{crack} · **W** · $C_{nocrack}$] · **InvW]**];

Print[MatrixForm[($C_{nocrack}$) · **Inverse[InvW +** D_{crack2} · **W** · $C_{nocrack}$] · **InvW]**];

```
Print[MatrixForm[(f1 C1 + f2 C2) . Inverse[InvW + Dcrack . W . Cnocrack] . InvW]];

Print[MatrixForm[A]];

Print[MatrixForm[distrain1]];

Print[MatrixForm[distrain2]];

Clear["Global`*"]; (* clears all variables from memory *)
```